

MOL #79137

Computational and experimental analysis of the TM4/TM5 dimerization interface of the serotonin 5-HT_{1A} receptor

**Nataliya Gorinski, Noga Kowalsman, Ute Renner, Alexander Wirth, Michael T. Reinartz,
Roland Seifert, Andre Zeug, Evgeni Ponimaskin, and Masha Y. Niv**

Cellular Neurophysiology, Medical School Hannover, Germany (N.G., A.W., A.Z., E.P.);

Institute of Biochemistry, Food Science and Nutrition, The Robert H Smith Faculty of
Agriculture, Food and Environment, and the Fritz Haber Center for Molecular Dynamics, the
Hebrew University of Jerusalem, Israel (N.K., M.Y.N);

DFG-Research Center for the Molecular Physiology of the Brain (CMPB), Göttingen, Germany
(U.R., E.P.);

Institute of Pharmacology, Medical School Hannover, Germany (M.T.R., R.S.)

MOL #79137

Running title: **5-HT_{1A} dimeric interface**

Corresponding author: Dr. Masha Niv, Institute of Biochemistry, Food Science and Nutrition and the Fritz Haber Center for Molecular Dynamics, the Hebrew University of Jerusalem, Israel, Tel.: (972)89489664; Fax.: (972)89476189; Email: niv@agri.huji.ac.il

Number of text pages: 56

Number of tables: 5

Number of figures: 7

Number of references: 70

Number of words in the *Abstract*: 249

Number of words in the *Introduction*: 658

Number of words in the *Discussion*: 1354

List of nonstandard abbreviations used in the paper: 3-dimensional (3D), 5-hydroxytryptamine (5-HT), cyan fluorescent protein (CFP), cytoplasmic membrane (CPM), dopamine D(2) receptor (D2), Förster resonance energy transfer (FRET), G-protein coupled receptor (GPCR), green fluorescence protein (GFP), intracellular loop (IL), molecular dynamics (MD), protein data bank (pdb), root mean square deviation (RMSD), root mean square fluctuation (RMSF), transmembrane (TM), van der Waals (vdW), wild-type (WT), yellow fluorescent protein (YFP), μ -opioid receptor (μ).

MOL #79137

ABSTRACT

Experimental evidence suggests that most members of class A G-protein coupled receptors (GPCRs) can form homomers and heteromers, in addition to functioning as single monomers. In particular, serotonin (5-HT) receptors were shown to homodimerize and heterodimerize with other GPCRs, although the details and the physiological role of the oligomerization has not yet been fully elucidated. Here we used computational modeling of the 5-HT_{1A} receptor monomer and dimer to predict residues important for dimerization. Based on these results we carried out rationally designed site-directed mutagenesis. The ability of the mutants to dimerize was evaluated using different FRET-based approaches. The reduced levels of acceptor photobleaching-FRET, and the lower number of monomers participating in oligomers, as assessed by lux-FRET, confirmed the decreased ability of the mutants to dimerize and the involvement of the predicted contacts (namely, W175^{4.64}, Y198^{5.41}, R151^{4.40} and R152^{4.41}) at the interface. This information was reintroduced as constraints for computational protein-protein docking, to obtain a high-quality dimer model. Analysis of the refined model as well as molecular dynamics simulations of wild-type (WT) and mutant dimers revealed compensating interactions in dimer composed of WT and W175A mutant. This provides an explanation for the requirement of mutations of W175^{4.64} in both homomers for disrupting dimerization. Our iterative computational-experimental study demonstrates that transmembrane domains TM4/TM5 can form an interaction interface in 5-HT_{1A} receptor dimers and indicates that specific amino acid interactions maintain this interface. The mutants and the optimized model of the dimer structure may be used in functional studies of serotonin dimers.

Introduction

The 5-hydroxytryptamine (5-HT, serotonin) system in the brain is involved in multiple processes, including regulation of neurogenesis, neuronal activity, as well as respiratory and cardiovascular control (Richter et al., 2003) and energy balance (Lam and Heisler, 2007).

Serotonin receptors, with the exception of the 5-HT₃ ion channel, belong to G-protein-coupled receptors (GPCRs), a large and diverse family of membrane proteins whose members participate in regulating cellular and physiological processes and represent key pharmacological targets. The 5-HT_{1A} receptor subtype is involved in processes such as the regulation of neurogenesis, temperature control and regulation of sleep. Particular interest in this receptor has been raised due to its involvement in regulating depression and anxiety states (Lesch and Gutknecht, 2004).

In the last decade it has become clear that many GPCRs may function as dimers or higher order oligomers (Albizu et al., 2010; Ganguly et al., 2011; Lohse, 2010; Rozenfeld and Devi, 2011; Woehler et al., 2009). Oligomerization has implications for trafficking, signaling, and pharmacology of many members of the GPCR family, but in many cases the functional implications of GPCR oligomerization still need to be delineated.

Recently we have demonstrated that 5-HT_{1A} receptors form homodimers at the plasma membrane (Kobe et al., 2008; Woehler et al., 2009). The analysis of 5-HT_{1A} receptor oligomerization dynamics by combined FRET approaches revealed that receptor stimulation results in accumulation of FRET-negative complexes rather than in dissociation of oligomers to monomers. The oligomerization of 5-HT_{1A} receptors was shown to be constitutive (Ganguly et al., 2011), with the oligomerization status independent of ligand stimulation, but enhanced due to acute (but not chronic) cholesterol depletion (Paila et al., 2011a). Despite these advances, and

MOL #79137

computational work on monomers (Paila et al., 2011b), the interaction interface of 5-HT_{1A} dimers is still not known, and is the focus of the current paper.

Almost every transmembrane (TM) domain within the GPCR has been suggested to mediate the dimeric interactions, but TM domains 4 and/or 5 have gained the most support as dimerization interfaces (Gonzalez-Maeso et al., 2008; Hu et al., 2012; Johnston et al., 2011). The TM4-TM5 interface is also compatible with images obtained via atomic force microscopy (Fotiadis et al., 2003), protein data bank (pdb) entry 1n3m.pdb. Specifically, the extracellular part of TM4 was found to be involved in oligomerization by site-directed cysteine cross-linking studies in D2 homodimers (Guo et al., 2003), in 5-HT_{2C} (Mancia et al., 2008) and in the yeast STE2 receptor (Wang and Konopka, 2009).

In the present study we aimed to establish a working model of the three dimensional structure of the complex. As a first step, we constructed 3D models of 5-HT_{1A} receptor monomer, as described for modeling of other GPCRs (Levit et al.; Yarnitzky et al., 2010).

The monomer models were fitted into the TM4/TM5 dimeric model of rhodopsin (1n3m.pdb). Based on analysis of the residues contributing to the dimeric interaction in these models, we designed dimerization-disrupting mutations. We then carried out site-directed mutagenesis and monitored the dimerization levels of the mutants using different FRET-based approaches. The confirmed interactions were introduced as constraints in protein-protein docking of monomers, and the optimized dimeric models were analyzed. The best model of WT dimer and the models of the mutant receptor dimers were submitted to molecular dynamics (MD) simulations. These simulations rationalize the mutagenesis results and provide a detailed view of the interaction interface. The results of our study *i*) confirmed the existence of the TM4/TM5 dimer interface for 5-HT_{1A}, *ii*) enabled us to refine the model of the dimer, and *iii*) provided pharmacologically

MOL #79137

intact, dimerization-impaired 5-HT_{1A} monomers, an important tool for further functional studies of 5-HT_{1A} receptor dimerization. After the completion of our work, a structure by Manglik and coworkers (Manglik et al., 2012) revealed that the μ -opioid receptor (μ) crystallizes as a two-fold symmetrical dimer through a four-helix bundle motif formed by transmembrane segments 5 and 6. The serotonin dimer proposed in the current work, is theoretically capable of co-existence with the opioid-like 5, 6 dimer.

Materials and Methods

Recombinant DNA procedures. The construction of 5-HT_{1A} receptors fused to different spectral variants of the green fluorescence protein (GFP) has been described previously (Renner et al., 2007). The mutagenesis of potential interaction sites within 5-HT_{1A} receptor was performed using site-directed mutagenesis kit (Stratagene) according to the manufacturer's protocol. The following primers were used: W136A/D140A, sense, 5'- GCG CTA GAC AGG TAC GCG GCA ATC ACC GCC CCT ATA GAC TAC GTG -3', antisense, 5'- CAC GTA GTC TAT AGG GGC GGT GAT TGC CGC GTA CCT GTC TAG CGC -3'; L159A/L166A, sense, 5'- GCG CTG ATC TCG GCC ACT TGG CTC ATT GGC TTT GCC ATC TCC ATC CC -3', antisense 5'- GGG ATG GAG ATG GCA AAG CCA ATG AGC CAA GTG GCC GAG ATC AGC GC-3'; W175A, sense, 5'-CGC CTA TGC TGG GCG CGC GCA CCC CGG AAG-3', antisense, 5'-CTT CCG GGG TGC GCG CGC CCA GCA TAG GCG-3'; R151K/R152K, sense 5'-CAA GAG GAC GCC CAA GAA GGC CGC TGC GCT GAT C-3', antisense, 5'-GAT CAG CGC AGC GGC CTT CTT GGG CGT CCT CTT G-3'; R176K, sense, 5'-GCC TAT GCT GGG CTG GAA GAC CCC GGA AGA CCG C, antisense, 5'- GCG GTC TTC CGG GGT CTT CCA GCC CAG CAT AGG C-3'; Y198F, sense, 5'-CGG GTA CAC CAT CTT CTC CAC TTT CGG CGC-3', antisense, 5'-GCG CCG AAA GTG GAG AAG ATG GTG TAC CCG-3'.

All mutants were verified by double-stranded dideoxy DNA sequencing at the level of the final plasmid.

Adherent cell culture and transfection. Mouse N1E-115 neuroblastoma cells from the American Type Culture collection (ATCC) were grown in Dulbecco's modified Eagle's medium (DMEM) containing 10% fetal calf serum (FCS) and 1% penicillin/streptomycin at 37°C under 5% CO₂. For transient transfection, cells were seeded at low-density in 60-mm dishes (1x10⁶) or

MOL #79137

on 10-mm cover-slips (5×10^5) and transfected with appropriate vectors using Lipofectamine2000 Reagent (Invitrogen) according to the manufacturer's instruction. Four hours after transfection, cells were serum starved over night before analysis. The amount of expressed receptor was measured in membrane preparations of transfected cells by using radioactive ligand binding assay with [3 H]8-OH-DPAT as a specific ligand and non-radioactive 5-HT as a competitor.

Expression and glycosylation of 5-HT_{1A} receptor WT and interaction interface mutates.

Twenty-four hours post-transfection cells were washed in PBS, lysed with 100 μ l Laemmli loading buffer, and 15 μ l of each sample were separated by 10% SDS-PAGE under reducing conditions. To analyse the glycosylation profile, lysates were prepared and treated with EndoH and PNGase F according to the manufacturer protocol (New England Biolabs). Briefly, cells transfected with yellow fluorescent protein (YFP)-tagged 5-HT_{1A} receptor were lysed in glycoprotein genaturating buffer and then treated with 1.000 units of corresponding glycosidase (EndoH or PNGase F) along with untreated controls for 1 h at 37°C. Finally samples were separated by 10% SDS-PAGE under reducing conditions. YFP or GFP-tagged constructs were visualized after SDS-PAGE directly in the gel by using variable mode imager Typhoon 9400 (GE Healthcare). For that, gels were excited at λ_{ex} 488 nm and emission was collected by using a band pass filter 530 BP 25.

Radioligand binding assay. Membrane preparation of transiently transfected N1E cells was performed as previously described (Renner et al., 2007) and stored at -80°C until used. For the competition binding assasy, membranes were thawed and re-suspended in binding buffer (75 mM Tris/HCl, 12.5 mM MgCl₂, 1 mM EDTA, pH 7.4) resulting in a final protein concentration of 0.72 $\mu\text{g}/\mu\text{L}$. Membranes were homogenized by using a 22-gauge needle (ten times) followed by a 27-gauge needle (15 times). Test tubes with a total reaction volume of 500 μL contained

MOL #79137

membranes with 18 μg of protein, 8-OH-DPAT (Tocris, Minneapolis, USA) at increasing concentrations, and [^3H]8-OH-DPAT (Hartmann Analytics; Braunschweig, Germany) at a final concentration of 1 nM. Reactions were shaken at 250 rpm at room temperature for 90 min in order to establish equilibrium. Separation of bound and free [^3H]8-OH-DPAT was achieved by filtration through Whatmann glass-fibre filters (grade GF/C, presoaked with 0.3% (v/v) polyethyleneimine in binding buffer) followed by three washing steps each with 2 mL of cold binding buffer using a 48-well Brandel harvester. Radioactivity was measured by liquid-scintillation-counting using Rotiszint eco plus cocktail (Carl Roth; Karlsruhe, Germany). Data were analyzed by non-linear regression functionality of PRISM 5.0 (GraphPad Software; La Jolla, CA, USA).

Confocal imaging and single-cell acceptor photobleaching FRET analysis. Images of N1E-115 cells expressing WT and different mutants of 5-HT_{1A}-CFP and 5-HT_{1A}-YFP fusion proteins were acquired with an LSM780-Meta confocal microscope (Carl Zeiss Jena) equipped with a 40x/1.3 NA oil-immersion objective at 512 x 512 pixels. The 458 nm line of a 40 mW argon laser was used at 15% power. Fluorescence emission was acquired from individual cells over 14 lambda channels, at 10.7 nm steps, ranging from 475 to 625 nm. For each measurement a series of 8 images was acquired over duration of 124 seconds. After the 4th image acquisition, bleaching of the acceptor (YFP) was performed in a selected 20 x 20 pixel region of interest in the plasma membrane. For that the 514 nm line of the Argon laser set at 50% power and 100% transmission for 300 scanning interactions using a 458nm/514nm dual dichroic mirror was used. Linear unmixing was performed by the Zeiss AIM software package using CFP and YFP reference spectra. Reference spectra were obtained from images of cells expressing only 5-HT_{1A}-

MOL #79137

CFP or 5-HT_{1A}-YFP acquired with acquisition settings mentioned above. Apparent FRET efficiency was calculated offline using the equation,

$$Ef_D = 1 - \left(\frac{F_{DA}}{F_D} \right) \quad (1)$$

where f_D is the fraction of donor participating in the FRET complex (*i.e.* ratio of FRET complexes over a total donor concentration, $[DA]/[D^t]$), F_{DA} and F_D are the background subtracted and acquisition bleaching corrected pre- and post-bleach CFP fluorescence intensities, respectively. The acquisition bleaching corrected post-bleach CFP intensities were calculated as

$$F_D = F_D^{B,post} + \left(\frac{F_D^{R,pre} - F_D^{R,post}}{F_D^{R,pre}} \right) F_D^{B,pre} \quad (2)$$

where F_D^B and F_D^R refer to CFP intensities of the bleach and reference region of interest, and *pre* and *post* refer to pre-bleach and post-bleach measurements.

Spectral lux-FRET analysis in living cells. Mouse N1E-115 neuroblastoma cells were co-transfected with plasmid DNAs encoding for WT and/or mutated 5-HT_{1A} receptors fused with CFP and YFP. Sixteen hours after transfection, cells were resuspended in PBS. All measurements were performed in 5 mm pathway quartz cuvettes using a spectrofluorometer (Fluorolog, Horiba JobinYvon) equipped with xenon lamp (450 W, 950V). The cell suspension was stirred with a magnetic stirrer while the temperature was maintained at 37°C during the experiment. For calibration measurements, cells were co-transfected with plasmid encoding a single fluorophore-tagged 5-HT_{1A} receptor together with an equal amount of plasmid encoding HA-tagged 5-HT_{1A} receptor. During the time-course experiments, two emission spectra were obtained for each time point by exciting at 458 nm and 488 nm with 5 nm spectral resolution for excitation and emission and 0.5 second integration time. The spectral contributions due to light

MOL #79137

scattering and non-specific fluorescence of the cells were taken into account by subtracting the emission spectra of non-transfected cells (background) from each measured spectra. Before each measurement, the spectrofluorometer was calibrated for the xenon-lamp spectrum and Raman scattering peak position.

To determine apparent FRET for WT and mutants of the 5-HT_{1A} receptor we used a recently developed method described in detail by Włodarczyk et al. (Włodarczyk et al., 2008). This allows for a calculation of the total concentration ratio $[A^t]/[D^t]$ of donor and acceptor, a donor molar fraction $x_D = [D^t]/([D^t]+[A^t])$ as well as the apparent FRET efficiencies Ef_D and Ef_A , where $f_D = [DA]/[D^t]$ and $f_A = [DA]/[A^t]$ are the fractions of donors and acceptors in complexes. A model characterizing apparent FRET efficiency, Ef_D , as a function of donor mole fraction, x_D , for oligomeric structures has been developed previously (Veatch and Stryer, 1977),

$$Ef_D = E(1 - x_d^{n-1}) \quad (3)$$

Fitting this model to experimental data allows for the estimation of the true transfer efficiency, E , and also provides information about the number of units, n , interacting in the oligomeric complex. Recently, this model has been slightly augmented for use with Ef_A , (Meyer et al., 2006),

$$Ef_A = E \frac{x_d}{1 - x_d} (1 - x_d^{n-1}) \quad (4)$$

Modeling the 5-HT_{1A} monomer. The mouse 5-HT_{1A} receptor sequence (accession #Q64264 see Supplemental Methods) was extracted from the UniProt server using the UniProtKB database. This sequence was used for modeling the 5-HT_{1A} monomers by two protein structure prediction automated servers: M4T (<http://manaslu.aecom.yu.edu/M4T/>) (Fernandez-Fuentes et al., 2007) and I-TASSER (<http://zhanglab.ccmb.med.umich.edu/I-TASSER/>) (Roy et al., 2010). M4T builds 3D models of proteins by comparative modeling using a combination of multiple

MOL #79137

templates and iterative optimization of alternative alignments. The output of M4T produced a single model that was used in this study (termed TRP_out1, in which W175^{4.64} pointed toward the outer surface of TM4). I-TASSER assembles 3D models based on multiple-threading alignments and iterative TASSER assembly simulations. I-TASSER returns up to 5 models. The model ranked 1 (best score) by I-TASSER was chosen as a monomer unit (termed TRP_in1, in which W175^{4.64} pointed into the TM-bundle) see Table 1. With the recent release of several new GPCR structures, we re-used both M4T and I-TASSER for creating new monomers. The top-ranking model from I-TASSER (termed TRP_in2, "in" and "out" nomenclature describing the W175 orientation), the third best model from I-TASSER (TRP_out3) and the M4T model (TRP_out2) were used in the subsequent analysis as well. The models are listed in Table 1, and the references for the GPCR templates used in their construction appear in the (Supplemental Methods).

Intracellular loop 3 (IL3) in 5-HT_{1A} receptor contains more than 100 residues (residues 218-345 as defined by the UniProtKB server). This is a unique feature of 5-HT_{1A} receptor compared with the rest of the 5-HT receptors. The protein disorder prediction for IL3 was predicted using the PrDOS (Protein DisOrder prediction System) server (Ishida and Kinoshita, 2007) <http://prdos.hgc.jp/cgi-bin/top.cgi>. The sequence of mouse IL3 (residues 218-345) was given as input to the server using default values. The output shows predictions of ordered and disordered regions in IL3 at a 5% false positive rate. Moreover, in the templates used for modeling the 5-HT_{1A} monomer (and other available GPCR structures) IL3 is either missing or replaced by the T4-lysozyme domain; hence, no appropriate template structure can be found for this loop, and the modeled structure of IL3 in the 5-HT_{1A} receptor models could not be considered reliable. Therefore, in our models, residues 233-330 were cut out and the remaining ends of IL3 were

MOL #79137

connected. The resulting short loop was refined using the loop refinement protocol in the Accelrys Software, Inc. Discovery-Studio 2.5 package using the default parameters.

Preliminary modeling of 5-HT_{1A} receptor homodimers. Homodimers of 5-HT_{1A} receptor were obtained by superposing the monomer model on the structure of a putative Rhodopsin dimer (1n3m) (Fotiadis et al., 2003; Liang et al., 2003). The superposition was done for the TM helices only and was based on sequence alignment of 5-HT_{1A} receptor and rhodopsin using the Accelrys Software, Inc. Discovery Studio 2.5 package. Sequence alignment of mouse 5-HT_{1A} receptor and rhodopsin was prepared using the alignment procedure of the UniProtKB server, which uses the ClustalW algorithm. The definitions of the TMs were taken from the UniProtKB server.

The homodimers were then analyzed for detecting important residues in the interface by the FastContact version 2.0 (<http://structure.pitt.edu/servers/fastcontact/>) (Camacho and Zhang, 2005) and COILCHECK (<http://caps.ncbs.res.in/coilcheck/>) (Alva et al., 2008) servers. The output of these servers lists the energy contribution of different residues in the interface to the interaction energy. For the refined dimers we also conducted an alanine scan using the Robetta server (<http://rosetta.bakerlab.org/alascansubmit.jsp>) (Kortemme et al., 2004).

A detailed analysis of the interactions that a specific residue creates in the dimer was conducted using Discovery Studio 2.5 binding site analysis "Draw Ligand Interactions" tool and the hydrogen-bond and aromatic interactions monitors. Models of dimers (either WT/WT or with combinations of mutated structures) were minimized using 500 Adopted Basis Newton-Raphson method (ABNR) steps. Next the interactions created by specific residues were analyzed. Default values were used besides the cutoff distance of H-bond that was changed to 3.5Å. The

MOL #79137

interactions that can be detected by this tool are aromatic-aromatic (π - π , sigma- π , cation- π), van-der Waals (vdW), hydrogen-bond, charged interaction (electrostatic), and polar.

The data about mutations in 5-HT receptors were extracted from the GPCRDB (<http://www.gpcr.org/7tm/>) (Vroling et al., 2011).

Refinement of the model.

Docking - Protein-protein docking was done using the program HADDOCK (High Ambiguity Driven protein-protein DOCKing) (<http://haddock.science.uu.nl/services/HADDOCK/haddock.php>) (De Vries et al., 2010). HADDOCK is an information-driven flexible docking approach for the modeling of biomolecular complexes. For each docking run, the same monomer (either TRP_out2, TRP_in2 or TRP_out3) was uploaded to the HADDOCK "easy interface" server as molecules A and B. Residues R151^{4.40}, R152^{4.41}, W175^{4.64}, R176^{4.65}, and Y198^{5.41} were defined as "Active residues (directly involved in the interaction)". The numbering in superscript 4.40, 4.41 etc. are in Ballesteros-Weinstein universal GPCR numbering, in which the most conserved position in TM X is denoted as X.50 and the other residues are numbered relative to it (Ballesteros and Weinstein, 1995). All the HADDOCK docking solutions are clustered and ranked according to their HADDOCK scores. The HADDOCK score is the weighted sum of van-der Waals, electrostatic, desolvation, and restraint violation energies, together with the buried surface area. As part of the scoring function (the "restraint violation energies") HADDOCK performs a number of violation analyses, including the number of times a restraint is violated and the average distance and violation per restraint. As output, the best scoring structures of each cluster can be downloaded or directly viewed. Fast manual inspection of the models allowed filtering of non-relevant models leaving only clusters of models in which the monomers are positioned correctly in the membrane. A representative of each resulting

MOL #79137

cluster of models was analyzed for the residues that contribute most to the interaction energy (using the FastContact (Camacho and Zhang, 2005), COILCHECK (Alva et al., 2008) and Robetta alanine scan servers (Kortemme et al., 2004)). Residues with $\Delta\Delta G > 2$ Kcal were regarded as hotspots. The dimer interface was analyzed using the PROTORP server <http://www.bioinformatics.sussex.ac.uk/protorp/> (Reynolds et al., 2009). PROTORP measures different interface physicochemical parameters such as the interface accessible surface area (interface size), the number of residues in the interface, the number of hydrogen bonds, gap-index and more (Reynolds et al., 2009).

Molecular Dynamics of WT and mutant 5-HT_{1A} homodimers - We created mutant dimers by mutating several residues on one or both monomers of the HADDOCK out3-out3 dimer using the Accelrys Software, Inc. Discovery Studio 2.5 mutagenesis tool.

These mutated dimers as well as the WT dimer were subjected to the leap Langevin simulated annealing refinement procedure in vacuum using the Chemistry at HARvard Macromolecular Mechanics (CHARMM) program (<http://www.charmm.org/>) (Brooks et al., 2009). The models underwent minimization of the 500 steepest-descent steps followed by 500 minimization Adopted Basis Newton-Raphson method (ABNR) steps prior to the simulated annealing. During the simulated annealing the models were heated from 100 to 300 degrees and were left at 300 degrees Kelvin for a production run of 15ns (5 fsec timestep).

Root mean square deviation (RMSD) analysis of the TMs in the trajectories was done using the CHARMM Corrmn RMS command. The TM definition was taken from the UniProtKB database (accession #Q64264). Root mean square fluctuation (RMSF) per residue was calculated using "rmsf-residue.str" CHARMM script created by Prof. Lennart Nilsson freely available at the script archive of the CHARMM forums. Residue RMSD per frame analysis was carried out

MOL #79137

using the VMD program (Humphrey et al., 1996) RMSD trajectory tool. Distance change during simulation was also calculated using VMD with a distance.tcl script from the VMD program script archive. All analyses were carried out on pre-aligned snapshots from the trajectories.

Defining 5-HT_{1A} putative binding site – we have defined the putative binding site of the 5-HT_{1A} in two ways: once using the ligand docking results (Yap et al., 2012), which listed the residues that are in direct contact with serotonin (S199^{5.42}, T200^{5.43} and D116^{3.32}) and pinolol (D116^{3.32}, I113^{3.29}, K191^{5.34} and N386^{7.39}). Secondly, we used analogy to dopamine D3 receptor (D3) Xray structure. For this purpose, we superposed the 5-HT_{1A} model TRP_out3 onto chain A of the D3 Xray structure 3pbl (Chien et al., 2010). The superposition was carried out for the TMs parts only, using the Accelrys Software, Inc. Discovery Studio 2.5 package superposition by sequence alignment tool. The alignment between the mouse 5-HT_{1A} and human D3 (accession #P35462) and the definition of the TMs in 5-HT_{1A} were taken from UniProtKB. We extracted the residues that are in direct contact with the eticlopride in 3pbl structure (figure 3 in (Chien et al., 2010)) and found the equivalent residues in 5-HT_{1A}. These were considered as the second definition of the binding site of 5-HT_{1A} (A93^{2.61}, D110^{3.32}, V111^{3.33}, F112^{3.28}, C114^{3.36}, I189, T196^{5.39}, S199^{5.42}, T200^{5.43}, A203^{5.46}, W342^{6.48}, F361^{6.51}, F362^{6.52}, A365^{6.55}, L366^{6.56}, T369^{7.39}, G382^{7.35}, Y390^{7.43}).

Comparing the putative 5-HT_{1A} dimer with the μ -opioid receptor dimer. We extracted the sequence of mouse μ -OR (accession #P42866) and 5-HT_{1A} and aligned them using UniProt. For the μ -OR dimer we have used the recently published structure 4dkl.pdb. We used the Protein interfaces, surfaces and assemblies service PISA (Krissinel and Henrick, 2007) to reproduce the dimer that was reported in (Manglik et al., 2012). Two 5HT_{1A} TRP_out3 monomer copies were superimposed on both molecules of the μ -OR dimer using Accelrys Software, Inc. Discovery

MOL #79137

Studio 2.5 package as described previously for the 5-HT_{1A} and the D3 dopamine receptor. 5-HT_{1A} residues that are equivalent to the interface residues of the μ -OR dimer were extracted based on the structure-based sequence alignment.

Sequence conservation analysis. Sequences of 5-HT_{1A} from different species and of other 5-HT₁ receptor subtypes were extracted from the UniProtKB database (Supplemental Methods). Sequence alignments of the 5-HT_{1A} in different species and of mouse 5-HT₁ receptor subtypes were prepared using the alignment procedure of the UniProtKB server, which uses the ClustalW algorithm.

MOL #79137

Results

Modeling of the 5-HT_{1A} receptor monomer. We used two servers, the M4T server (Fernandez-Fuentes et al., 2007), and the I-TASSER server (Roy et al., 2010) to construct several 3D models of the 5-HT_{1A} receptor, since there is no experimental structure of a monomer of 5-HT_{1A} or any other serotonin receptor. We repeated the modeling of the monomer, in the course of this work, as experimental structures continued to appear. The main difference between the different 5-HT_{1A} models is the location of residues W175^{4.64} and R176^{4.65}. In some of the models (termed here TRP_in1, TRP_in2, etc.), the Trp residue W175^{4.64} points into the TM bundle, whereas R176^{4.65} points towards a potential dimeric interface (see Fig. 1A and B). In other models, termed TRP_out1, TRP_out2, etc., W175^{4.64} residue points out into the dimeric interface and R176^{4.65} points into the TM bundle. Table 1 lists the monomers prepared for this study. For each monomer, the server that created it and the GPCR templates used for its preparation are shown. The models are similar to each other, with a TM backbone RMSD (root mean square deviation) of 1.39Å between models TRP_out1 and TRP_in1. The TM RMSD between the M4T TRP_out1 and TRP_out2 models is 1.25Å and an RMSD of 1.20Å between the I-TASSER TRP_in1 and TRP_in2, and 1.68Å between the TRP_in1 and TRP_out3 models. A unique feature of 5-HT_{1A} is that its IL3 is particularly long: it contains more than 100 residues (residues number 218-345) and is predicted to be partially disordered (see Materials and Methods). In experimentally determined GPCR structures IL3 is either missing or replaced by T4-lysozyme domain. Therefore, the IL3 loop of the 5-HT_{1A} receptor models is not expected to be reliably modeled, and was shortened, as described in Materials and Methods.

Modeling the 5-HT_{1A} receptor homodimers. Data from atomic force microscopy maps of rhodopsin in its native disk membrane was used for proposing a 3D molecular model of a GPCR

MOL #79137

oligomer (Fotiadis et al., 2003) This model showed an arrangement of rhodopsin molecules in 2-dimensional (2D) arrays of dimers. In this arrangement, TM4, TM5 and the intracellular loop (IL) connecting TM3 and TM4 (IL2) are involved in intradimeric interactions, whereas TM1, TM2 and the intracellular loop connecting TM5 and TM6 (IL3) are involved in interdimeric interactions. We hypothesized that the dimeric organization in 5-HT_{1A} receptors is similar to that proposed for the rhodopsin (Liang et al., 2003; Niv and Filizola, 2007) and dopamine receptors (Guo et al., 2005).

The copies of the monomer models TRP_in and TRP_out were superposed on the structure of the rhodopsin dimer (chains A and C in 1n3m.pdb). The corresponding resulting dimer models, in-dimer and out-dimer, were manually inspected and submitted to servers that estimate protein-protein interaction energies, such as COILCHECK (Alva et al., 2008) and FastContact (Camacho and Zhang, 2005). The residues that either contribute most to the interaction energy in the out-dimers (an example can be seen in (Supplemental Tables 1 and 2)) or that are potentially important for the dimerization based on manual inspection are: W136^{3.52} and D140^{3.56} in IL2 loop, L159^{4.48}, L166^{4.55}, and W175^{4.64} in TM4 or in the beginning of EL2 and Y198^{5.41} in TM5 (see Fig. 1A). D140^{3.56} and W136^{3.52} interact with R151^{4.40}, which has been shown to be important for signaling (Kushwaha et al., 2006).

In the TRP-in dimer the residues that contribute most to the interaction are similar (Supplemental Tables 1 and 2): W136^{3.52}, D140^{3.56}, L166^{4.55} and Y198^{5.41}. The main difference is that in the out-dimer W175^{4.64} turns into the predicted dimeric interface, whereas in the in-dimer R176^{4.65} turns into the interface instead of W175^{4.64} (as shown in Fig. 1A and B). Consequently, W175^{4.64} is predicted to contribute to the energy of the interactions in the out-dimers but not in the in-dimers. A representative structure of the out-dimer and the residues discussed above are schematically

MOL #79137

shown in Fig. 1C. Since both dimer models, TRP_in and TRP_out, are valid, both models were next used for suggesting mutations that may disrupt dimerization.

Design, expression, and glycosylation of mutants in the proposed interface. Based on the 5-HT_{1A} homodimers model described above, mutations within the predicted interaction interface were designed to disrupt or weaken the dimerization interface (Table 2). The positive charge at the end of the TMs is important for correctly inserting the helix into the membrane (Lerch-Bader et al., 2008). Therefore, in residues R151^{4.40}, R152^{4.41} and R176^{4.65} we mutated the positively charged Arg into positively charged Lys, which is shorter and creates fewer interactions. In other cases, such as residues W136^{3.52}, D140^{3.56}, L159^{4.48} and L166^{4.55}, we carried out the conventional mutagenesis into an Ala residue. Y198^{5.41} was mutated to Phe, a minimal perturbation that can test the importance of hydrogen bonding at this position. Several mutations were combined to increase the potential effect of the construct on the dimerization.

To analyse the expression of substitution mutants, they were fused to different spectral variants of GFP and expressed in neuroblastoma N1E-115 cells, followed by SDS-PAGE and fluorescence analysis. Fig. 2A demonstrates that the WT and all mutants were expressed at similar levels, and were detectable as a double protein band. We hypothesized that the double bands shown in Fig. 2A for all constructs represent differently glycosylated receptor species. To test this hypothesis, the WT construct and the mutants were treated with glycopeptidase F (PNGase-F), an enzyme that removes all types of N-linked carbohydrates. This treatment resulted in a single protein band shifted to approximately 55 kDa, as expected for the fusion construct without any additional modifications, confirming that the two protein bands were indeed caused by different glycosylation (Fig. 2B). Treatment of probes with endoglycosidase H (endo-H), which removes only carbohydrates of the high mannose type, revealed that the upper

MOL #79137

protein band is not shifted and hence contain processed carbohydrates. In contrast, the lower species shift to the same position as the PNGase-F-treated protein and therefore contain unprocessed carbohydrates of the high mannose type (Fig. 2B). Attachment of unprocessed carbohydrates of the high mannose type occurs in the endoplasmic reticulum (ER), whereas terminal glycosylation takes place in the trans-Golgi and represents an important signal for transporting receptors to the plasma membrane.

In order to characterize a precursor-product relationship for various receptor mutants, the intensities of the upper (processed) and the lower (unprocessed) protein bands were compared. As shown in Fig. 2C, the upper/lower band ratio for the W175A, R176K, Y198F, L159A/L166A and R176K/Y198F mutants was similar to that obtained for the WT receptor, suggesting their correct processing and transport to the plasma membrane. The ratio was slightly decreased with the R151K/R152K mutant (suggesting that this mutant had higher retention in the ER, as was predicted for several mutations in R151 including R151K (Kushwaha et al., 2006)). In contrast, the ratio was significantly decreased in the R151K/R152K/Y198F, W136A/D140A, and W136A/D140A/R151K/R152K mutants, suggesting their predominant localization in the ER. Taken together, these results indicate that most, but not all, of the 5-HT_{1A} receptor mutants undergo complete processing and can therefore be targeted to the cytoplasmic membrane (CPM).

Subcellular distribution of mutant. We next analyzed the subcellular distribution of mutants in order to detect their exact localization in the cells. Confocal microscopy performed after transfection of WT 5-HT_{1A}-YFP constructs into N1E-115 cells indicated that most of the receptors were present on the plasma membranes and only a minor fraction of them was present in the intracellular compartments (Fig. 3). For the W175A, R176K, Y198F, R176K/Y198F,

MOL #79137

L159A/L166A and R151K/R152K mutants, we obtained a similar distribution, which is also consistent with the glycosylation data (Fig. 2C). In contrast, the membrane localization was lost for the R151K/R152K/Y198F, W136A/D140A and W136A/D140A/R151K/R152K mutants, and these proteins were homogeneously distributed within the cytoplasm (Fig. 2C and Table 2).

These combined data indicate that the W175A, R176K, Y198F, R176K/Y198F, L159A/L166A and R151K/R152K mutants possess biochemical features as well as subcellular distributions similar to the WT 5-HT_{1A} receptor, whereas others have modified distributions.

Modified cellular distribution of GPCR mutants is a well documented phenomenon, which may occur naturally, sometimes causing pathologies (Pulagam and Palczewski, 2010), or in site-directed mutagenesis (Milligan, 2009). We return to this issue in the Discussion, whereas the rest of this work focuses on mutants that localize at the plasma membrane: W175A, R176K, Y198F, R151K/R152K, L159A/L166A, and R176K/Y198F.

Pharmacological analysis of mutants. Having demonstrated the plasma membrane localization of W175A, R176K, Y198F, R151K/R152K, L159A/L166A, and R176K/Y198F mutants, we next analyzed whether their pharmacological properties are affected. Pharmacological profiling of the wild-type and mutated receptors by competitive binding of the radioactively-labelled agonist [³H]8-OH-DPAT and non-radioactive 8-OH-DPAT revealed no significant differences among the receptor constructs (Fig. 4). The IC₅₀ values calculated for mutants were also similar to the IC₅₀ WT 5-HT_{1A} receptor (Table 3). These results are in line with the predicted ligand binding site, which was expected to be affected by the mutation (Supplemental Figure 1). Notably, the pharmacological results obtained in the present study are in line with published data on the recombinant 5-HT_{1A} receptor in membrane preparations of CHO cells, where logIC₅₀ of -

MOL #79137

8.42 ± 0.06 for the wild-type receptor was calculated (Khawaja et al., 1997). Thus, all membrane localized mutants possess the same pharmacological properties as the 5-HT_{1A} receptor wild-type.

Analysis of 5-HT_{1A} receptor oligomerization using acceptor photobleaching FRET. We have recently established a confocal microscopy-based acceptor photobleaching FRET assay to demonstrate the oligomerization of the 5-HT_{1A} receptor at the single-cell level (Kobe et al., 2008). In the present study this method was applied to compare the oligomerization efficiency of the WT and the five plasma membrane localized mutants that were designed to have impaired receptor oligomerization. Neuroblastoma N1E-115 cells were transfected with 5-HT_{1A}-CFP (donor) and 5-HT_{1A}-YFP (acceptor) fusion constructs in different combinations, and receptors expressed in the plasma membrane (Fig. 5A) were analyzed for interaction. To avoid artifacts resulting from overexpression, we adjusted the total expression level for the CFP- and YFP-tagged receptor to 1.000-1.200 fmol/mg proteins in all the following FRET experiments, which allows for quantitative analysis of results obtained in different experiments. Moreover, a similar amount of endogenous 5-HT_{1A} receptors was obtained in the hippocampus under physiological conditions (Hoyer et al., 1986).

Fig. 5B shows the bleached region of interest with a loss of YFP intensity as well as a reference region of interest from which the acquisition bleaching rate was determined for corrected FRET calculation. In the bleached region of interest the loss of acceptor fluorescence was accompanied by increased donor emission intensity that is characteristic of FRET. In contrast, the intensities of both CFP and YFP fluorescence in non-bleached regions undergo only minor decreases (acquisition bleaching).

Finally, the apparent FRET efficiency, E_{fD} , was calculated (Eq. 1 and 2). Data were background subtracted and corrected for acquisition bleaching using the measurements from the reference

MOL #79137

region of the plasma membrane (Fig. 5C). The WT receptor fusion proteins from cells with similar donor (CFP) to acceptor (YFP) ratios were found to have a mean apparent FRET efficiency of $18.9 \pm 0.6 \%$, which is in accordance with our previous results (Kobe et al., 2008). After expression of CFP- and YFP-tagged W175A and R151K/R152K mutants, FRET efficiency was significantly reduced to $12 \pm 0.7 \%$ and $11.9 \pm 0.6 \%$, respectively. Also co-expression of W175A with either the R176K or Y198F mutants resulted in a decrease of FRET signal to $12 \pm 0.7 \%$ and $13 \pm 1 \%$, respectively. Double mutant R176K/Y198F presented on both monomers reduces the FRET efficiency to $13.5 \pm 1.3\%$. In contrast, FRET efficiency was not changed when R176K-CFP and R176K-YFP or Y198F-CFP and Y198F-YFP combinations were analyzed. Similarly, combining WT with either W175A, Y198F, or R176K mutants, as well as co-expression of R176K with Y198F, or W175A with R151K/R152K did not influence the FRET efficiency (Fig. 5C).

These data suggest that W175^{4.64} residues from different monomers are involved in forming the interaction interface. Tryptophan at position 175^{4.64} can also interact with R176^{4.65} and Y198^{5.41} located on the opposite monomer to stabilize the receptor complex. In addition, interactions of both R176^{4.65} and Y198^{5.41} with R176^{4.65} and Y198^{5.41} residues on the opposite monomer may contribute to dimerization eventhough a single mutation is not enough to disrupt it. These results provide a stronger support to the TRP_out models than the TRP_in model (Fig. 1). Another important region of dimerization is likely to be formed by residues R151^{4.40} and R152^{4.41}, which can interact with the corresponding amino acids on the opposite monomer.

No decrease in dimerization was found for combinations of either WT or mutant constructs with the L159A/L166A mutant. These results indicate that R159^{4.48} and L166^{4.55} are probably not pivotal for maintaining the binding interaction between the two 5-HT_{1A} monomers.

MOL #79137

Analysis of 5-HT_{1A} receptor dimerization by the lux-FRET. The apparent FRET efficiency, Ef_D , measured by the acceptor photobleaching is inherently dependent on f_D , the fraction of donor participating in FRET complexes. This is in turn dependent upon the ratio of total donor concentration $[D_t]$ to total acceptor concentration $[A_t]$ present in the sample. It has been suggested that the dependence of Ef_D on $[A_t]/[D_t]$ may be useful in differentiating FRET resulting from specific vs. random interactions (James et al., 2006). In the case of random interaction, Ef_D has been predicted to be independent of the total donor to acceptor ratio at a fixed surface density above a certain ratio. Therefore, we next calculated the apparent FRET-efficiencies for donors, Ef_D , and acceptors, Ef_A , over a wide range of donor molar fraction, x_D ($x_D = [D^t]/([D^t]+[A^t])$). For that we applied quantitative linear unmixing FRET (lux-FRET) method, which allows determining all aforementioned parameters (Włodarczyk et al., 2008). Using the lux-FRET approach we have previously demonstrated the specificity of 5-HT_{1A} receptor oligomerization (Kobe et al., 2008; Woehler et al., 2009) and performed detailed analysis of the 5-HT_{1A} oligomerization behaviour in living cells (Renner et al.). In the present study, we applied the lux-FRET method to quantify apparent FRET efficiency as a function of donor/acceptor ratio for wild-type and mutated 5-HT_{1A} receptors. To be able to perform quantitative comparison of FRET values obtained at different donor to acceptor ratios, the total concentration of plasmids encoding for donor and acceptor was held constant in all experiments. Graphs shown in Fig. 6 clearly demonstrate functional dependence of both Ef_D and Ef_A from the donor molar fraction, x_D , thus confirming specific receptor-receptor interaction. Based on the lux-FRET analysis we also estimated the number of units participating in complex, n (Eq. 3 and 4) and obtained a best fit for the value of $n = 2.2$ ($R^2=0.94$, Fig. 6A) for the 5-HT_{1A} receptor wild-type. The goodness of fit was similar in the range from $n = 2.1$ to $n = 2.3$ (Supplemental

MOL #79137

Figure 2). After co-expression of the WT-YFP (acceptor) with W175A-CFP (donor), the n -values reside at a similar range ($n = 2.0$, $R^2=0.97$, Fig. 6B), and the maximal R^2 values were obtained for n ranged from 1.9 to 2.1 (Supplemental Figure 2). In contrast, after co-expression of W175A-CFP with W175A-YFP n -value was lowered to $n = 1.4$ ($R^2=0.95$, Fig. 6C and Supplemental Figure 2)). The co-expression of W175A-CFP (donor) with Y198F-YFP (acceptor) also resulted in decreasing the n value, to n ranged from 1.3 to 1.5 ($R^2=0.90$; Supplemental Figure 2)). These results indicate that amount of receptors existing in monomeric form was increased after expression of the W175A mutant or after co-expression of W175A with Y198F mutant, when compared with the WT receptors (expressed either alone or in combination with W175A). Taken together, these data confirm the importance of amino acids W175^{4,64} and Y198^{5,41} in forming the dimeric complex.

Refinement of the model. Anchor-driven simulated annealing molecular dynamics was successfully used to predict peptide interactions with homology models of PDZ domains (Niv and Weinstein, 2005) and to incorporate experimental constraints into an activated model of rhodopsin (Niv et al., 2006). Here we used the restraints-driven protein-protein docking tool HADDOCK (De Vries et al., 2010) to dock two protomer copies of either TRP_out2, TRP_in2 or TRP_out3, using constraints as described next.

The results of our experimental procedures indicated that the W175A mutation decreases oligomerization, when placed in both (but not in a single) monomers. R176K placed in both monomers does not influence dimerization, but the combination of R176K in one monomer with W175A in the other monomer decreases dimerization. This suggests interaction between W175^{4,64} and R176^{4,65}. Mutant Y198F alone or in combination with R176K does not influence

MOL #79137

dimerization, but W175A in combination with Y198F reduces dimerization. This suggests the existence of interaction between W175^{4.64} and Y198^{5.41}.

In summary, our experimental results indicate interactions between W175^{4.64} in one monomer with W175^{4.64}, R176^{4.65} and Y198^{5.41} in the other monomer, possibly simultaneously. In addition, mutations R151K/R152K placed in both monomers decrease dimerization.

The residues R151^{4.40}, R152^{4.41}, W175^{4.64}, R176^{4.65} and Y198^{5.41} were used as constraints in HADDOCK (De Vries et al., 2010) by defining them as "active residues" (residues directly involved in the interaction). A default docking run resulted in up to 200 refined putative solutions. These solutions were clustered based on their structural similarity, as measured by RMSD (clustering details described in Materials and Methods section). Parameters for representative models in each cluster, such as the HADDOCK energy score and its components (Van der Waals energy, electrostatic energy, desolvation energy, and the penalty energy due to violation of restraints), the number of models in the cluster and the interface size (the buried surface area in both monomers Å²), were reported (Table 4).

Representative structures in the resulting clusters of docking solutions were inspected manually for the general positioning of the monomers with respect to each other and to the membrane. In the docking solutions of TRP_out2 monomers, no representative models passed the manual inspection and were not analyzed further. For docking solutions of TRP_in2 monomers (termed in2-in2), the first cluster of the docked models contained 55 structures, from which a representative, well-behaved model, was obtained. In the rest of the clusters, the monomers were not positioned well with respect to each other and to the membrane. The docking solutions of the TRP_out3 monomer resulted in one cluster, consisting of all of the 200 models. The parameters for the top-ranked structure in each cluster are presented in Table 4.

MOL #79137

To compare these refined, constraint-driven models (in2-in2 and out3-out3), with the preliminary models that we obtained by superimposing the monomers on a 1n3m.pdb template (TRP_out2-dimer, TRP_in2-dimer and TRP_out3-dimer; Fig. 1), we assessed the models using PROTORG server (Reynolds et al., 2009). PROTORG is a bioinformatics tool designed to analyze the interfaces between soluble protein chains in protein-protein complexes by calculating a set of physicochemical parameters exhibited by each protein interface. To the best of our knowledge, no analogous analysis has yet been done in membrane proteins. With this caveat in mind, Table 5 presents part of the interface properties that were measured. These measures are commonly used for identifying true vs. false interfaces. For example, the average interface area per monomer calculated for 122 homodimers was found to be 1940\AA^2 , the average number of residues in the interface was 52, and the average number of H-bonds was 9 (Bahadur et al., 2003). In addition, the monomers in real interfaces usually have good complementarity. One way to evaluate the complementarity of the monomers in the interface is the gap index. A lower gap index indicates higher complementarity (Jones and Thornton, 1996). Judging by their larger interface, with a higher number of residues in the interface, and a higher number of hydrogen or electrostatic contacts, the monomers are positioned better in the refined HADDOCK models than in the preliminary 1n3m-based models. In-silico alanine scanning, using the Robetta alanine scan server (Kortemme et al., 2004), was performed as an additional evaluation measure. No hotspots were predicted in any of the preliminary dimers, whereas for the refined models the Robetta server predicted both W175^{4.64} and Y198^{5.41} to be hotspots. Among the two HADDOCK models, the out3-out3 dimer has better values both in its HADDOCK cluster parameters (Table 4) and in most PROTORG parameter values (Table 5). For example, the cluster that includes the best putative model is significantly larger and the HADDOCK score for the top-ranking model is

MOL #79137

better; this model's interface size approaches the average homodimers' interface sizes, and it has a higher number of residues in the interface. The number of interactions is similar for the two models (Table 4), but the HADDOCK out3-out3 dimer has fewer gaps than does the HADDOCK in2-in2 dimer.

The superior quality of the out3-out3 model is in accord with the experimental results mentioned earlier, which indicated that W175^{4,64} is located at the interface, as is the case in the out3-out3, but not in the in2-in2 dimer. Based on these combined data, out3-out3 was chosen as the best current model of the dimer. Fig. 7A gives a general overview of the out3_out3 dimer.

Rationalizing the data obtained for the receptor mutants. Several combinations of mutations were experimentally shown to decrease the dimerization. Interestingly, a mutation on one of the monomers only, did not significantly reduce the dimerization. This indicates that mutants were still capable of maintaining strong interactions with the WT. We aimed at understanding the detailed structural and molecular reasons underlying these observations. The fine-tuned HADDOCK out3-out3 dimer now enables such a detailed analysis of the interactions in the interface (Fig. 7B and C).

We analyzed the contacts created by residues W175^{4,64} and Y198^{5,41} using the WT dimer and the mutant dimers (Supplemental Table 3). In the WT dimer, residue W175^{4,64} of both monomers creates aromatic-aromatic (π - π) interactions with each other. In addition each of them (I:W175 and II:W175) is involved in vdW interactions with Y198^{5,41} on the opposite monomer (Fig. 7C and (Supplemental Table 3)). W175^{4,64} on both molecules is indeed predicted to be the strongest hotspot in the Robetta alanine scan (Kortemme et al., 2004). It is therefore not surprising that when W175^{4,64} is mutated in both monomers the dimerization decreases significantly. The analysis of the contacts also reveals that there are no contacts made by the mutated W175A

MOL #79137

residues. Interestingly, when only one W175^{4.64} is mutated, the dimerization ability is only marginally lowered (Fig. 5C). This can be explained by the fact that in the WT/W175A dimer model, the vdW interaction still exists between the mutant W175A and WT W175^{4.64}. Alternatively, W175^{4.64} on the WT monomer can still interact with Y198^{5.41} of the mutated monomer which, in turn, can move to create even stronger interactions with Y198^{5.41}.

The Y198^{5.41} residue was also predicted to be a hotspot by the alanine-scan. Indeed, in the WT out3-out3 dimer model, Y198^{5.41} is involved in several interactions, including hydrogen-bond between the OH groups of the I:Y198 and II:Y198 and interaction with W175^{4.64} in the opposite monomer (Fig. 7C). When Y198^{5.41} is mutated to Phe in one monomer, it loses the hydrogen bond with the Y198 on the opposite monomer but it can still create most of the WT interactions. However, when W175^{4.64} is mutated to Ala in monomer I (I:W175A) and Y198^{5.41} to Phe in monomer II (II:Y198F), the interface loses both the aromatic interaction between I:W175 and II:W175 and the hydrogen bond between the Y198^{5.41} residues. In addition, the mutated residues W175A and Y198F cannot create compensating interactions in the way that Y198 and W175 probably do in the WT/W175A and W175A/WT combinations. We deduce that the aromatic interactions created by W175^{4.64} with W175^{4.64}, the interaction between W175^{4.64} and Y198^{5.41} on opposite monomers, and the hydrogen bond between I:Y198 and II:Y198 (Fig. 7C and (Supplemental Table 3)) have a pivotal effect on the total interaction energy of the dimerization.

The interactions involving R151^{4.40} and R152^{4.41} in our model are not strong enough to explain their pivotal role in the interface, as seen in the FRET experiments (Supplemental Table 3).

To further investigate the role of R151^{4.40} and R152^{4.41} in dimerization, specific interacting residues should be identified. Our models suggested that they may interact with residues from IL2 in the other monomer, such as W136^{3.52} and D140^{3.56}. However, W136A/D140A double

MOL #79137

mutant 5-HT_{1A} constructs did not reach the plasma membrane (Fig. 2, 3 and Table 2) and therefore we could not test this hypothesis. The refined 5-HT_{1A} models suggest an additional residue as a candidate for interacting with R151^{4.40} and R152^{4.41}, namely, D143^{3.59}. The refined model not only predicts D143^{3.59} to be in the interface but it also suggests that this residue may have high contribution to the binding energy.

Using the initial computational dimer model we have predicted several residues on the surface of 5-HT_{1A} to be important for 5-HT_{1A} dimerization. The experimental procedures have shown that indeed some of these residues are pivotal for the dimerization and this data allowed fine-tuning of the 5-HT_{1A} homodimer model. The resulting fine-tuned 5-HT_{1A} homodimer model provides detailed information about these interactions.

To evaluate the robustness of our conclusions, we subjected the WT HADDOCK out3-out3 dimer and several combinations of mutants (WT with II:W175A, I:W175A with II:W175A, WT with II:Y198F and I:Y198F with II:W175A) to 15ns MD simulation. To see the effect of a more pronounced mutation in residue Y198^{5.41}, we also carried out an MD simulation of the WT/II:Y198A combination although this mutation was not generated experimentally. The trajectories were analyzed with focus on the behavior of residues 175^{4.64}, 176^{4.65} and 198^{5.41} on both monomers. The overall stability of the monomers and the dimers was examined by manual inspection and TMs C α RMSD monitoring during the run analysis. In 5 out of 6 unrelated WT/WT runs the overall structure of the monomers and dimers remained stable during the simulation. The average RMSD of the TMs stabilized after a few nsec (Supplemental Figure 3). Residue root mean square fluctuation (RMSF) analysis also suggested that the structures are stable (data not shown).

MOL #79137

In the WT/Y198A MD simulation the RMSD of the TM C α increases throughout the simulation as opposed to the TM C α RMSD of the WT/Y198F. Interestingly, the change is due to one of the monomers tilting with respect to the other monomer and to the membrane. Since such a change is not feasible within a realistic membrane, this may suggest that in the realistic membrane the stability of this dimer is reduced compared with the WT.

We obtained decreased dimerization in W175A/W175A and W175A/Y198F combinations of mutants, while the combination WT/W175A did not impair the dimerization. We hypothesized that in the WT/W175A combination the remaining I:W175 that cannot interact with the mutated II:W175A may strengthen its interaction with II:Y198 whereas II:Y198 maintains its interaction with I:Y198, thus keeping the interface intact. An analysis of the distances between the aromatic rings of I:W175 and II:Y198 during the WT/WT and WT/WT175A MD simulation supported our hypothesis. In the absence of II:W175, residue I:W175 moves closer to II:Y198, whereas the distance between I:Y198 II:Y198 does not change (Supplemental Figure 4).

MOL #79137

Discussion

It is now widely accepted that GPCRs can form oligomers, and a growing body of evidence points to the functional importance of oligomeric complexes for receptor trafficking, receptor activation and G-protein coupling in native tissues (Rivero-Muller et al., 2010). The clinical significance of GPCR oligomerization has also become more evident during recent years, leading to identification of receptor oligomers as novel therapeutic targets (Gonzalez-Maeso et al., 2008; Waldhoer et al., 2005). However, the lack of detailed structural information for GPCR dimers still raises an important challenge of understanding the functional role of oligomerization. Therefore, during the last decade efforts were made to create models of GPCRs and their dimers by the use of computational simulations (Casciari et al., 2008; Filizola and Weinstein, 2005; Johnston and Filizola, 2011; Simpson et al., 2010) resulting in working models and testable hypotheses.

In the present work we have combined computational and experimental procedures in order to investigate the 5-HT_{1A} homodimerization. We have focused on the interaction interface within TM4 and TM5 and identified specific residues that are involved in the interaction between two monomeric units. Interestingly, the rationally designed mutations resulted in significantly decreased dimerization, but did not completely prevent receptor-receptor interaction. This is in accord with the assumption that the 5-HT_{1A} receptor can form higher-order oligomers (Ganguly et al., 2011). In this case interface-disrupting mutations interfere only with one interface, while allowing interaction between two monomers on the other interface. Future investigation of additional interfaces will contribute to better understanding of the 5-HT_{1A} oligomerization behavior.

MOL #79137

Cellular distribution of the mutant 5-HT_{1A} receptors. It was important to identify those mutated receptors that were localized at the plasma membrane to ensure that the receptors used in our study are mature, did not undergo structural deformation and do not produce artifacts due to crowded environment. Indeed, some of the designed 5-HT_{1A} receptor mutants did not reach the plasma membrane, but rather remained in the intracellular compartments such as ER and/or Golgi (*e.g.* W136A/D140A; Table 2 and Fig. 2 and 3). Modified cellular distribution of GPCR mutants is important feature to receptor regulation and signalling (Jean-Alphonse and Hanyaloglu, 2011). Interestingly, several natural mutations of GPCRs that have pathophysiological implications also cause receptor retention within intracellular compartments (Bulenger et al., 2005). It has been shown that changing the hydrophobicity profile of residues, in particular Asp from the transmembrane region, can affect the transverse position of a corresponding TM helix and as a consequence affect the receptor distribution within the cell (Krishnakumar and London, 2007). Similar changes in the hydrophobicity profile may explain the disrupted membrane localization of the D140A mutant observed in the current work. We focused our studies on properly distributed mutants only.

Identified interface residues and comparison to other family A GPCRs. We have identified residues involved in the interfaces between the 5-HT_{1A} receptor monomers. Noteworthy that some of these residues were previously mentioned to play a role in regulation of the 5-HT receptor functions. For example, the effect of T190^{4.40} residue in 5-HT_{2A} receptor on agonist induced receptor desensitization was described (Gray et al., 2003). In the case of the 5-HT_{1A} receptor, R151^{4.40} and R152^{4.41} residues were suggested to be involved in the G-protein coupling (Kushwaha et al., 2006). Since these residues participate in receptor-receptor interaction interface, it will be interesting to study whether the decreased G-protein coupling obtained by

MOL #79137

Kushwaha et al. (Kushwaha et al., 2006) is due to impaired dimerization. To the best of our knowledge, residues R151^{4.40}, R152^{4.41}, W175^{4.64} and Y198^{5.41} were found for the first time to be involved in dimerization of 5-HT receptors and not to be involved in ligand binding. 5.41 flanking residues, such as S199^{5.42} in the 5-HT_{1A} receptor (Ho et al., 1992) and I199^{5.40} in the 5-HT_{1D} receptor (Wurch et al., 1998), were shown to be involved in ligand binding. This is in agreement with our structural model, where both W175^{4.64} and Y198^{5.41} point to the dimerization interface and not into the binding pocket. R176^{4.65} does point into the upper part of the TM core but it is not part of the binding site as defined either by (Yap et al., 2012) or by analogy to D3-dopamine receptor binding site (Chien et al., 2010) see (Supplemental Figure 1).

Interestingly, in δ -opioid receptor (δ) homodimeric complexes investigated by bioluminescence resonance energy transfer (BRET), cross-linking and MD simulations, residue A163^{4.40}, which is equivalent to R151 in the 5-HT_{1A} receptor, has been shown to take part in the proposed TM4 and TM4/TM5 interfaces, while K164^{4.41}, which is equivalent to R152 in the 5-HT_{1A} receptor, participates in the proposed TM4/TM5 interface only. In contrast, residue C216^{5.41}, which is equivalent to Y198 in the 5-HT_{1A} receptor, does not participate in the dimeric interfaces (Johnston et al., 2011).

After the completion of our current study, the structure of μ -opioid receptor (Manglik et al., 2012) joined the increasing numbers of structures of GPCRs in this exciting and ground breaking era of X-ray crystallography (Katritch et al., 2012; Sprang, 2011; Steyaert and Kobilka, 2011). The μ -opioid receptor molecules are associated into pairs along the crystallographic two-fold axis through two different interfaces. One of the interfaces involves TM5 and TM6 and buried surface area of 1,492Å². This interface is suspected to be of biological relevance (Manglik et al., 2012). Interestingly, we find that three monomers of serotonin may, in principle, bind

MOL #79137

simultaneously, presenting both the μ -opioid receptor-like TM5/TM6 interface and the TM4/TM5 interface (analyzed in the current work), because there are no significant clashes in such an arrangement (Supplemental Figure 5). It is therefore possible that in high-order oligomers both interfaces may take part.

Mutagenesis of both monomers. Our experimental results showed that in some cases, mutations of both monomers are needed in order to disrupt dimerization. We hypothesized that compensating interaction may occur between the mutant and the WT protomers, but not in the mutant dimer. We used *in-silico* mutagenesis and *in-vacuo* 15 nsec MD simulations to test this hypothesis. Indeed, the simulations provided possible explanations for the experimental results, *i.e.* in WT and W175A mutant dimerization, the distance between the remaining I:W175 residue and II:Y198 residue decreases after a few nanoseconds. This results in better positioning between the residues and allows stronger interactions. These suggestions will be tested in the future in experimental work and using additional simulation techniques, including explicit solvent, enhanced sampling and free energy simulations (Johnston and Filizola, 2011).

Relevance of findings to other organisms and other 5-HT₁ subtypes. The amino acid sequence of the 5-HT_{1A} receptor is highly conserved between species. In particular, R151^{4.40}, R152^{4.41}, R176^{4.65} and Y198^{5.41}, that were found to be important for dimerization in the current work, are fully conserved in 18 representative species (including mammals, fish and reptiles). Interestingly, W175^{4.64} is conserved in 15 out of the 18 species tested. Three fish sequences having a Met residue instead of W175^{4.64} also have an insertion in EL2 (Supplemental Figure 6). If 5-HT_{1A} receptors in these species homodimerize, this might be achieved by a compensation for absence of W175^{4.64} by interactions from the EL2 loop insertion. The residues we found to be pivotal for the 5-HT_{1A} receptor dimerization, are conserved also in other 5-HT₁ receptor

MOL #79137

subtypes: W175^{4.64}, R176^{4.65} and Y198^{5.41}. At position 4.40 (5-HT_{1A} R151) there is a positively charged residue in four out of the five 5-HT₁ sequences. At position 4.41 (5-HT_{1A} R152) there is an Arg residue in 5-HT_{1A}, _{1B} and _{1E}) while in 5-HT_{1D} and 5-HT_{1F} there is a His residue which may also be positively charged (Supplemental Figure 7). These results indicate a possibility for heterodimerization between different 5-HT₁ subtypes, which should be further investigated.

In summary, our work supports the transmembrane domains TM4/TM5 as the interface involved in dimerization of the 5-HT_{1A} receptor. Residues W175^{4.64}, Y198^{5.41}, R151^{4.40} and R152^{4.41} were computationally predicted and experimentally confirmed to be important for the interaction interface. Since the 5-HT_{1A} mutants designed and characterized in this work show significantly reduced dimerization, they can be utilized to investigate the functional importance of the 5-HT_{1A} receptor dimerization. This will aid in studying the role of dimerization in 5-HT_{1A} signal transduction and facilitate further studies of 5-HT_{1A} oligomerization and heterodimerization of 5-HT_{1A} with other receptors.

MOL #79137

Acknowledgments

We thank Dr. Talia Yarnitzky for helpful discussions.

Authorship Contributions.

Participated in research design: Kowalsman, Ponimaskin, Seifert and Niv.

Conducted experiments: Gorinski, Kowalsman, Renner, Wirth, Reinartz, Zeug and Niv.

Contributed new reagents or analytic tools: Zeug

Performed data analysis: Kowalsman, Gorinski, Zeug, Reinartz, Ponimaskin and Niv.

Wrote or contributed to the writing of the manuscript: Kowalsman, Ponimaskin and Niv.

MOL #79137

References

- Albizu L, Cottet M, Kralikova M, Stoev S, Seyer R, Brabet I, Roux T, Bazin H, Bourrier E, Lamarque L, Breton C, Rives ML, Newman A, Javitch J, Trinquet E, Manning M, Pin JP, Mouillac B and Durroux T (2010) Time-resolved FRET between GPCR ligands reveals oligomers in native tissues. *Nat Chem Biol* **6**(8): 587-594.
- Alva V, Devi DPS and Sowdhamini R (2008) COILCHECK: An interactive server for the analysis of interface regions in coiled coils. *Protein Pept Lett* **15**(1): 33-38.
- Bahadur RP, Chakrabarti P, Rodier F and Janin J (2003) Dissecting subunit interfaces in homodimeric proteins. *Proteins* **53**(3): 708-719.
- Ballesteros J and Weinstein H (1995) Integrated methods for the construction of three-dimensional models and computational probing of structure-function relations in G protein-coupled receptors *Methods in Neurosci* **25**: 366–428.
- Brooks BR, Brooks CL, III, Mackerell AD, Jr., Nilsson L, Petrella RJ, Roux B, Won Y, Archontis G, Bartels C, Boresch S, Caflisch A, Caves L, Cui Q, Dinner AR, Feig M, Fischer S, Gao J , Hodoscek M, Im W, Kuczera K, Lazaridis T, Ma J, Ovchinnikov V, Paci E, Pastor RW, Post CB, Pu JZ, Schaefer M, Tidor B, Venable RM, Woodcock HL, Wu X, Yang W, York DM and Karplus M (2009) CHARMM: The Biomolecular Simulation Program. *J Comput Chem* **30**(10): 1545-1614.
- Bulenger S, Marullo S and Bouvier M (2005) Emerging role of homo- and heterodimerization in G-protein-coupled receptor biosynthesis and maturation. *Trends Pharmacol Sci* **26**(3): 131-137.
- Camacho CJ and Zhang C (2005) FastContact: rapid estimate of contact and binding free energies. *Bioinformatics* **21**(10): 2534-2536.

MOL #79137

- Casciari D, Dell'Orco D and Fanelli F (2008) Homodimerization of neurotensin 1 receptor involves helices 1, 2, and 4: insights from quaternary structure predictions and dimerization free energy estimations. *J Chem Inf Model* **48**(8): 1669-1678.
- Chien EYT, Liu W, Zhao Q, Katritch V, Han GW, Hanson MA, Shi L, Newman AH, Javitch JA, Cherezov V and Stevens RC (2010) Structure of the Human Dopamine D3 Receptor in Complex with a D2/D3 Selective Antagonist. *Science* **330**(6007): 1091-1095.
- De Vries SJ, van Dijk M and Bonvin AMJJ (2010) The HADDOCK web server for data-driven biomolecular docking. *Nat Protoc* **5**(5): 883-897.
- Fernandez-Fuentes N, Rai BK, Madrid-Aliste CJ, Eduardo Fajardo J and Fiser A (2007) Comparative protein structure modeling by combining multiple templates and optimizing sequence-to-structure alignments. *Bioinformatics* **23**(19): 2558-2565.
- Filizola M and Weinstein H (2005) The study of G-protein coupled receptor oligomerization with computational modeling and bioinformatics. *FEBS J* **272**(12): 2926-2938.
- Fotiadis D, Liang Y, Filipek S, Saperstein DA, Engel A and Palczewski K (2003) Atomic-force microscopy: Rhodopsin dimers in native disc membranes. *Nature* **421**(6919): 127-128.
- Ganguly S, Clayton AHA and Chattopadhyay A (2011) Organization of Higher-Order Oligomers of the Serotonin1A Receptor Explored Utilizing Homo-FRET in Live Cells. *Biophys J* **100**(2): 361-368.
- Gonzalez-Maeso J, Ang RL, Yuen T, Chan P, Weisstaub NV, Lopez-Gimenez JF, Zhou M, Okawa Y, Callado LF, Milligan G, Gingrich JA, Filizola M, Meana JJ and Sealfon SC (2008) Identification of a serotonin/glutamate receptor complex implicated in psychosis. *Nature* **452**(7183): 93-97.
- Gray JA, Compton-Toth BA and Roth BL (2003) Identification of two serine residues essential for agonist-induced 5-HT2A receptor desensitization. *Biochemistry* **42**(36): 10853-10862.
- Guo W, Shi L, Filizola M, Weinstein H and Javitch JA (2005) Crosstalk in G protein-coupled receptors: changes at the transmembrane homodimer interface determine activation. *Proc Natl Acad Sci USA* **102**(48): 17495-17500.

MOL #79137

- Guo W, Shi L and Javitch JA (2003) The fourth transmembrane segment forms the interface of the dopamine D2 receptor homodimer. *J Biol Chem* **278**(7): 4385-4388.
- Ho BY, Karschin A, Branchek T, Davidson N and Lester HA (1992) The role of conserved aspartate and serine residues in ligand binding and in function of the 5-HT1A receptor: a site-directed mutation study. *FEBS Lett* **312**(2-3): 259-262.
- Hoyer D, Pazos A, Probst A and Palacios JM (1986) Serotonin receptors in the human brain. I. Characterization and autoradiographic localization of 5-HT1A recognition sites. Apparent absence of 5-HT1B recognition sites. *Brain Res* **376**(1): 85-96.
- Hu J, Thor D, Zhou Y, Liu T, Wang Y, McMillin SM, Mistry R, Challiss RA, Costanzi S and Wess J (2012) Structural aspects of M3 muscarinic acetylcholine receptor dimer formation and activation. *FASEB J* **26**(2): 604-616.
- Humphrey W, Dalke A and Schulten K (1996) VMD: visual molecular dynamics. *J Mol Graph* **14**(1): 33-38.
- Ishida T and Kinoshita K (2007) PrDOS: prediction of disordered protein regions from amino acid sequence. *Nucleic Acids Res* **35**: W460-W464.
- James JR, Oliveira MI, Carmo AM, Iaboni A and Davis SJ (2006) A rigorous experimental framework for detecting protein oligomerization using bioluminescence resonance energy transfer. *Nat Methods* **3**(12): 1001-1006.
- Jean-Alphonse F and Hanyaloglu AC (2011) Regulation of GPCR signal networks via membrane trafficking. *Mol Cell Endocrinol* **331**(2): 205-214.
- Johnston JM, Aburi M, Provasi D, Bortolato A, Urizar E, Lambert NA, Javitch JA and Filizola M (2011) Making Structural Sense of Dimerization Interfaces of Delta Opioid Receptor Homodimers. *Biochemistry* **50**(10): 1682-1690.
- Johnston JM and Filizola M (2011) Showcasing modern molecular dynamics simulations of membrane proteins through G protein-coupled receptors. *Curr Opin Struct Biol* **21**(4): 552-558.

MOL #79137

- Jones S and Thornton JM (1996) Principles of protein-protein interactions. *Proc Natl Acad Sci USA* **93**(1): 13-20.
- Katritch V, Cherezov V and Stevens RC (2012) Diversity and modularity of G protein-coupled receptor structures. *Trends Pharmacol Sci* **33**(1): 17-27.
- Khawaja X, Ennis C and Minchin MC (1997) Pharmacological characterization of recombinant human 5-hydroxytryptamine1A receptors using a novel antagonist radioligand, [3H]WAY-100635. *Life Sci* **60**(9): 653-665.
- Kobe F, Renner U, Woehler A, Wlodarczyk J, Pampusheva E, Bao G, Zeug A, Richter DW, Neher E and Ponimaskin E (2008) Stimulation- and palmitoylation-dependent changes in oligomeric conformation of serotonin 5-HT1A receptors. *Biochim Biophys Acta* **1783**(8): 1503-1516.
- Kortemme T, Kim DE and Baker D (2004) Computational alanine scanning of protein-protein interfaces. *Sci STKE* **2004**(219): pl2.
- Krishnakumar SS and London E (2007) The control of transmembrane helix transverse position in membranes by hydrophilic residues. *J Mol Biol* **374**(5): 1251-1269.
- Krissinel E and Henrick K (2007) Inference of macromolecular assemblies from crystalline state. *J Mol Biol* **372**(3): 774-797
- Kushwaha N, Harwood SC, Wilson AM, Berger M, Tecott LH, Roth BL and Albert PR (2006) Molecular determinants in the second intracellular loop of the 5-hydroxytryptamine-1A receptor for G-protein coupling. *Mol Pharmacol* **69**(5): 1518-1526.
- Lam DD and Heisler LK (2007) Serotonin and energy balance: molecular mechanisms and implications for type 2 diabetes. *Expert Rev Mol Med* **9**(5): 1-24.
- Lerch-Bader M, Lundin C, Kim H, Nilsson I and von Heijne G (2008) Contribution of positively charged flanking residues to the insertion of transmembrane helices into the endoplasmic reticulum. *Proc Natl Acad Sci USA* **105**(11): 4127-4132.

MOL #79137

- Lesch KP and Gutknecht L (2004) Focus on The 5-HT_{1A} receptor: emerging role of a gene regulatory variant in psychopathology and pharmacogenetics. *Int J Neuropsychopharmacol* **7**(4): 381-385.
- Levit A, Barak D, Behrens M, Meyerhof W and Niv MY Homology model-assisted elucidation of binding sites in GPCRs. *Methods in Mol Biol* **accepted**.
- Liang Y, Fotiadis D, Filipek S, Saperstein DA, Palczewski K and Engel A (2003) Organization of the G protein-coupled receptors rhodopsin and opsin in native membranes. *J Biol Chem* **278**(24): 21655-21662.
- Lohse MJ (2010) Dimerization in GPCR mobility and signaling. *Curr Opin Pharmacol* **10**(1): 53-58.
- Mancia F, Assur Z, Herman AG, Siegel R and Hendrickson WA (2008) Ligand sensitivity in dimeric associations of the serotonin 5HT_{2c} receptor. *EMBO Rep* **9**(4): 363-369.
- Manglik A, Kruse AC, Kobilka TS, Thian FS, Mathiesen JM, Sunahara RK, Pardo L, Weis WI, Kobilka BK and Granier S (2012) Crystal structure of the micro-opioid receptor bound to a morphinan antagonist. *Nature* **485**(7398): 321-326.
- Meyer BH, Segura JM, Martinez KL, Hovius R, George N, Johnsson K and Vogel H (2006) FRET imaging reveals that functional neurokinin-1 receptors are monomeric and reside in membrane microdomains of live cells. *Proc Natl Acad Sci USA* **103**(7): 2138-2143.
- Milligan G (2009) G protein-coupled receptor hetero-dimerization: contribution to pharmacology and function. *Br J Pharmacol* **158**(1): 5-14.
- Niv MY and Filizola M (2007) Influence of oligomerization on the dynamics of G-protein coupled receptors as assessed by normal mode analysis. *Proteins* **71**(2): 575-586.
- Niv MY, Skrabanek L, Filizola M and Weinstein H (2006) Modeling activated states of GPCRs :the rhodopsin template. *J Comput Aided Mol Des* **20**(7-8): 437-448.
- Niv MY and Weinstein H (2005) A flexible docking procedure for the exploration of peptide binding selectivity to known structures and homology models of PDZ domains. *J Am Chem Soc* **127**(40): 14072-14079.

MOL #79137

- Paila YD, Kombrabail M, Krishnamoorthy G and Chattopadhyay A (2011a) Oligomerization of the serotonin(1A) receptor in live cells: a time-resolved fluorescence anisotropy approach. *J Phys Chem B* **115**(39): 11439-11447.
- Paila YD, Tiwari S, Sengupta D and Chattopadhyay A (2011b) Molecular modeling of the human serotonin(1A) receptor: role of membrane cholesterol in ligand binding of the receptor. *Mol Biosyst* **7**(1): 224-234.
- Pulagam LP and Palczewski K (2010) Electrostatic compensation restores trafficking of the autosomal recessive retinitis pigmentosa E150K opsin mutant to the plasma membrane. *J Biol Chem* **285**(38): 29446-29456.
- Renner U, Glebov K, Lang T, Papusheva E, Balakrishnan S, Keller B, Richter DW, Jahn R and Ponimaskin E (2007) Localization of the mouse 5-hydroxytryptamine(1A) receptor in lipid microdomains depends on its palmitoylation and is involved in receptor-mediated signaling. *Mol Pharmacol* **72**(3): 502-513.
- Renner U, Zeug A, Woehler A, Niebert M, Dityatev A, Dityateva G, Gorinski N, Guseva D, Abdel-Galil D, Fröhlich M, Döring F, Wischmeyer E, Richter DW, Neher E and Ponimaskin EG Heterodimerization of serotonin receptors 5-HT1A and 5-HT7 differentially regulates receptor signalling and trafficking. *J Cell Sci* **accepted**.
- Reynolds C, Damerell D and Jones S (2009) ProtorP: a protein-protein interaction analysis server. *Bioinformatics* **25**(3): 413-414.
- Richter DW, Manzke T, Wilken B and Ponimaskin E (2003) Serotonin receptors: guardians of stable breathing. *Trends Mol Med* **9**(12): 542-548.
- Rivero-Muller A, Chou YY, Ji I, Lajic S, Hanyaloglu AC, Jonas K, Rahman N, Ji TH and Huhtaniemi I (2010) Rescue of defective G protein-coupled receptor function in vivo by intermolecular cooperation. *Proc Natl Acad Sci USA* **107**(5): 2319-2324.

MOL #79137

- Roy A, Kucukural A and Zhang Y (2010) I-TASSER: a unified platform for automated protein structure and function prediction. *Nature Protoc* **5**(4): 725-738.
- Rozenfeld R and Devi LA (2011) Exploring a role for heteromerization in GPCR signalling specificity. *Biochem J* **433**(1) 11-18.
- Simpson LM, Taddese B, Wall ID and Reynolds CA (2010) Bioinformatics and molecular modelling approaches to GPCR oligomerization. *Curr Opin Pharmacol* **10**(1): 30-37.
- Sprang SR (2011) Cell signalling: Binding the receptor at both ends. *Nature* **469**(7329): 172-173.
- Steyaert J and Kobilka BK (2011) Nanobody stabilization of G protein-coupled receptor conformational states. *Curr Opin Struct Biol* **21**(4): 567-572.
- Veatch W and Stryer L (1977) The dimeric nature of the gramicidin A transmembrane channel: conductance and fluorescence energy transfer studies of hybrid channels. *J Mol Biol* **113**(1): 89-102.
- Vroling B, Sanders M, Baakman C, Borrmann A, Verhoeven S, Klomp J, Oliveira L, de Vlieg J and Vriend G (2011) GPCRDB: information system for G protein-coupled receptors. *Nucleic Acids Res* **39**: D309-D319.
- Waldhoer M, Fong J, Jones RM, Lunzer MM, Sharma SK, Kostenis E, Portoghese PS and Whistler JL (2005) A heterodimer-selective agonist shows in vivo relevance of G protein-coupled receptor dimers. *Proc Natl Acad Sci USA* **102**(25): 9050-9055.
- Wang HX and Konopka JB (2009) Identification of Amino Acids at Two Dimer Interface Regions of the alpha-Factor Receptor (Ste2). *Biochemistry* **48**(30): 7132-7139.
- Wlodarczyk J, Woehler A, Kobe F, Ponimaskin E, Zeug A and Neher E (2008) Analysis of FRET signals in the presence of free donors and acceptors. *Biophys J* **94**(3): 986-1000.
- Woehler A, Wlodarczyk J and Ponimaskin EG (2009) Specific oligomerization of the 5-HT1A receptor in the plasma membrane. *Glycoconj J* **26**(6): 749-756.

MOL #79137

Wurch T, Colpaert FC and Pauwels PJ (1998) Chimeric receptor analysis of the ketanserin binding site in the human 5-hydroxytryptamine(1D) receptor: Importance of the second extracellular loop and fifth transmembrane domain in antagonist binding. *Mol Pharmacol* **54**(6): 1088-1096.

Yap BK, Buckle MJ and Doughty SW Homology modeling of the human 5-HT(1A), 5-HT (2A), D1, and D2 receptors: model refinement with molecular dynamics simulations and docking evaluation. *J Mol Model* **accepted**.

Yarnitzky T, Levit A and Niv MY (2010) Homology modeling of G-protein-coupled receptors with X-ray structures on the rise. *Curr Opin Drug Discov Devel* **13**(3): 317-325.

MOL #79137

FOOTNOTES:

Nataliya Gorinski and Noga Kowalsman are equally contributing authors.

This work was funded by the Niedersachsen-Israel research fund [grant ZN2448] and Deutsche Forschungsgemeinschaft DFG [grant PO732].

For reprint requests please contact Dr. Masha Niv, Institute of Biochemistry, Food Science and Nutrition and the Fritz Haber Center for Molecular Dynamics, the Hebrew University of Jerusalem, Israel, Tel.: (972)89489664; Fax.: (972)89476189; Email: niv@agri.huji.ac.il

MOL #79137

Figure legends:

Fig. 1: A general model of 5-HT_{1A} receptor monomer with residues predicted to participate in the dimer interaction interface. (A) Comparison between models TRP_out (left) and TRP_in (right). The monomers are shown as a cartoon green ribbon with emphasis on TM3, 4, and 5. The residues that are predicted to participate in the dimerization interface are represented as a CPK (Corey-Pauling-Koltun space filling) of their C α atom. These residues are positioned similarly along TMs 3-5, with the only significant difference arising for W175^{4.64} and R176^{4.65}; in TRP_out, W175^{4.64} faces the interface, whereas R176^{4.65} does not, and in TRP_in this situation is exactly the opposite. (B) A closer look at the difference between TRP_out (left) and TRP_in (right) monomers showing residues W175^{4.64} and R176^{4.65} in stick representation. (C) A cartoon of the out-dimer. The coloring of monomer I is the same as in (A) and (B). Monomer II is depicted in gray.

Fig. 2. Expression and glycosylation of 5-HT_{1A} receptor wild-type and substitution mutants. (A) Analysis of different YFP-tagged 5-HT_{1A} receptor constructs transiently expressed in neuroblastoma N1E-115 cells. The SDS-PAGE gel was scanned at λ_{ex} 488 nm, and emission was collected by using a band pass filter 530/25. The molecular weight marker is indicated on the left. (B) The 5-HT_{1A} receptor was digested with endo-H, PNGase-F or left untreated prior to SDS-PAGE and detection. Representative scans for 5-HT_{1A} WT are shown. (C) The precursor-product relationship of the WT and mutants plotted as the intensity ratio of the upper to the lower protein bands that are shown in (A). Data points represent the means \pm SEM from at least three independent experiments.

MOL #79137

Fig. 3: Subcellular distribution of the 5-HT_{1A} receptor wild-type and mutants. Representative confocal images of YFP-tagged receptors obtained with a LSM780-Meta microscope at 63x magnification are shown. Scale bar, 10 μ M.

Fig. 4: [³H]8-OH-DPAT competition binding at various 5HT_{1A} receptor mutants. Membranes of N1E-115 cells expressing either wild-type or plasma membrane localized 5HT_{1A} receptor mutants (18 μ g total protein) were subjected to the competition binding by incubation with 1nM [³H]8-OH-DPAT along with increasing concentrations of non-radioactive 8-OH-DPAT. Data are shown as mean \pm SD. Data were analyzed by non-linear regression and fitted to monophasic competition isotherms.

Fig. 5: Acceptor photobleaching FRET analysis of 5-HT_{1A} dimerization. (A) Confocal microscopy was used to visualize 5-HT_{1A}-CFP and 5-HT_{1A}-YFP co-expressed in the plasma membrane of N1E-115 cells. Fluorescence spectra were collected and unmixed for CFP and YFP components using the Zeiss LSM780-Meta detector. The fluorescence image of the CFP channel (green), the YFP channel (red), and composite channel before and after bleaching are shown. Box 1 corresponds to the bleached regions of interest (ROI), whereas box 2 corresponds to the non-bleached ROI. Scale bar, 10 μ m. (B) Enlargement of box 1 is shown in upper panel on the left. The 12-bit grayscale intensities of YFP and CFP during the whole trial are plotted for the bleached ROI (right). Enlargement of box 2 is shown in lower panel on the left. The 12-bit grayscale intensities of YFP and CFP during the whole trial are plotted for the non-bleached ROI (right). (C) The apparent FRET efficiency, E_{fD} , was calculated according to Eqs. 1 and 2. Data

MOL #79137

are shown as mean \pm SEM. **, $p < 0.01$. Mutations with significantly reduced Ef_D values are underlined.

Fig. 6: Oligomerization of 5-HT_{1A} receptor wild-type and mutants investigated by the lux-FRET. Apparent FRET efficiencies Ef_D (blue) and Ef_A (red) were calculated according to (Włodarczyk et al., 2008) and are shown as functions of the donor mole fraction x_D for the wild-type homomers (A), wild-type-W175A heteromers (B) as well as for the W175A homomers (C). Experimental data were fitted according to Eqs. 3 and 4, where n represents a number of units participating in complex. Data points represent the mean \pm S.E.M. of the apparent FRET efficiency values from at least 3 independent experiments

Fig. 7: The dimer and interface interactions in the HADDOCK out3-out3 dimer. (A) Good complementarity between the monomers in the HADDOCK TRP_out3-dimer. The monomers are shown in surface representation. Monomer I is shown in green and II in purple. The interface between the monomers is large and continuous (without many gaps). (B) A top 3D view of residues I:W175^{4.64} (left) and I:Y198^{5.41} (right) and the residues from monomer II that interact with them are shown. The residues are shown in green stick representation for monomer I and in purple stick representation for monomer II. Monomer I is shown in green and II in purple, both are shown as ribbons. (C) A cartoon representation of the residue I:W175^{4.64}, left, and I:Y198^{5.41}, right, and their interacting residues in molecule II. I:W175^{4.64} and I:Y198^{5.41} are shown in stick representation. The carbon atoms are in green, oxygen in red and nitrogen in light purple. The interacting residues from monomer II are represented by their C α atoms as colored spheres and their colors represent the interaction type with the color coding marked in the figure outline. The

MOL #79137

distances in Å between the C α atoms of the residues in monomer II and the closest carbon atom in either W175^{4.64} or Y198^{5.41} are shown in gray.

MOL #79137

Tables:

Table 1: The 5-HT_{1A} models used in this study. The table show for each model the server that was used for preparing it. The "+" sign is used to designate early and subsequent models that were created after the appearance of additional GPCR Xray structures in 2009. The references for the papers describing the template structures appear in (Supplemental Methods).

	TRP_out1	TRP_out2	TRP_out3	TRP_in1	TRP_in2
Created by server	M4T	M4T	I-TASSER	I-TASSER	I-TASSER
Early [2009, 2010]	+			+	
Subsequent [end of 2010, 2011]		+	+		+
PDB codes of templates used [references detailed in (Supplemental Methods)]	2rh1	2rh1, 3d4s 3eml	3pbl, 2rh1, 3ny8, 3eml	2rh1, 3d4s, 3eml	3pbl, 2rh1, 3ny8, 3eml

MOL #79137

Table 2: List of the 5-HT_{1A} mutated constructs tested in this study and their cellular localization.

Mutation	Region	Intracellular localization
W136A/D140A	IL3	ER/Golgi
R151K/R152K	IL3	Plasma membrane
L159A/L166A	TM4	Plasma membrane
W175A	TM4-EL2	Plasma membrane
R176K	EL2	Plasma membrane
Y198F	TM5	Plasma membrane
W136A/D140A/R151K/R152K	IL3	ER/Golgi
R176K/Y198F	TM4 and TM5	Plasma membrane
R151K/R152K/Y198F	IL3 and TM5	ER/Golgi

MOL #79137

Table 3: LogIC₅₀ values of [³H]8-OH-DPAT competition binding at various 5HT_{1A} receptor mutants. Data shown in Fig. 4 were analyzed by non-linear regression and fitted to monophasic competition isotherms to obtain logIC₅₀ values ± SD for 8-OH-DPAT for each receptor mutant. Pairwise comparison of the Gaussian-distributed logIC₅₀ values using one-way analysis of variance followed by Bonferroni's t-test showed no significant differences between the wild-type and all mutants tested.

5HT_{1A} receptor mutation	logIC₅₀ ± SD	IC₅₀ / nM (95% confidence interval)
Wild-type	-8.50 ± 0.07	3.18 (2.23 – 4.53)
W175A	-8.38 ± 0.06	4.14 (3.04 – 5.63)
R176K	-8.38 ± 0.06	4.17 (3.22 – 5.40)
Y198F	-8.50 ± 0.06	3.19 (2.34 – 4.35)
R176K/Y198F	-8.51 ± 0.07	3.06 (2.23 – 4.20)
R151K/R152K	-8.32 ± 0.10	4.77 (2.96 – 7.69)

MOL #79137

Table 4: HADDOCK scoring and evaluation of the in2-in2 and out3-out3 dimers suggest that out3-out3 is preferable to in2-in2 model. HADDOCK final score, the size of the cluster, the average backbone RMSD from the lowest energy structure of the cluster, Van der Waals, electrostatic and desolvation energies and the buried surface area in the dimer are shown for top cluster of two models.

Parameter	in2-in2 dimer	out3-out3 dimer
Monomer	TRP_in2	TRP_out3
HADDOCK score	-118.7 +/- 3.1	-239.5 +/- 5.7
Cluster size	55	200
RMSD from the overall lowest-energy structure in the cluster	29.0 +/- 0.9	1.1 +/- 0.8
Van der Waals energy	-46.5 +/- 3.2	-93.0 +/- 10.1
Electrostatic energy	-14.7 +/- 21.2	-73.0 +/- 20.5
Desolvation energy	-69.3 +/- 9.1	-136.7 +/- 8.9
Restraint violation energy	1.0 +/- 1.00	48.2 +/- 13.28
Buried surface area	1604.1 +/- 235.7	2859.6 +/- 103.4

MOL #79137

Table 5: PROTORP values for interface parameters in different 5-HT_{1A} dimer models suggest the out3-out3 as the optimal model.

	<i>TRP_out2- dimer</i>	<i>TRP_in2- dimer</i>	<i>TRP_out3- dimer</i>	<i>HADDOCK in2-in2</i>	<i>HADDOCK out3-out3</i>
Monomer	TRP_out2	TRP_in2	TRP_out3	TRP_in2	TRP_out3
Interface area on one monomer (Å²)	475.10	654.74	325.64	814.40	1478.17
Number of residues	19	19	18	23	37
Interactions (H- bonds and electrostatic)	6	4	0	12	11
Gap index	-	-	-	4.72	1.59

Figure 1

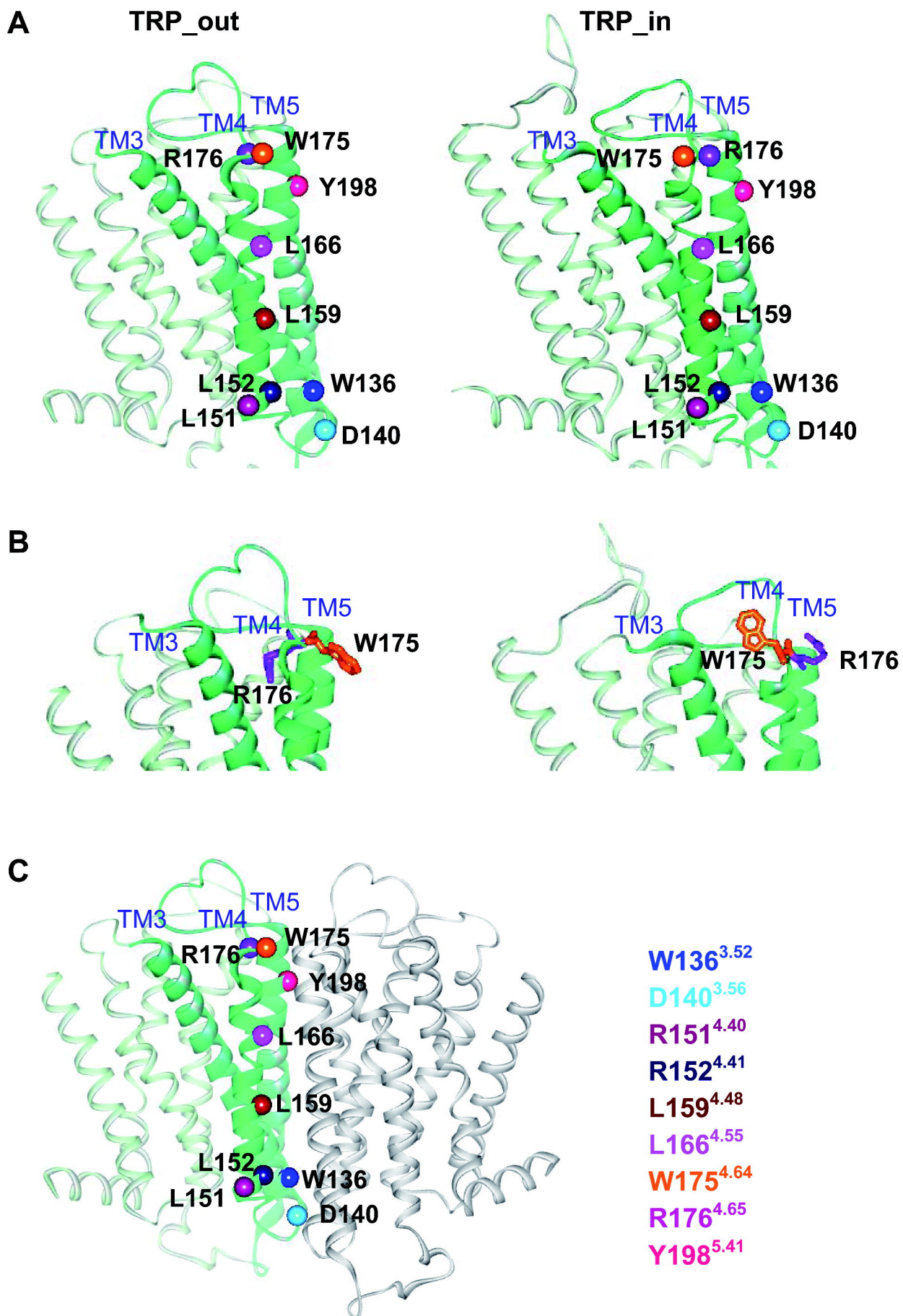
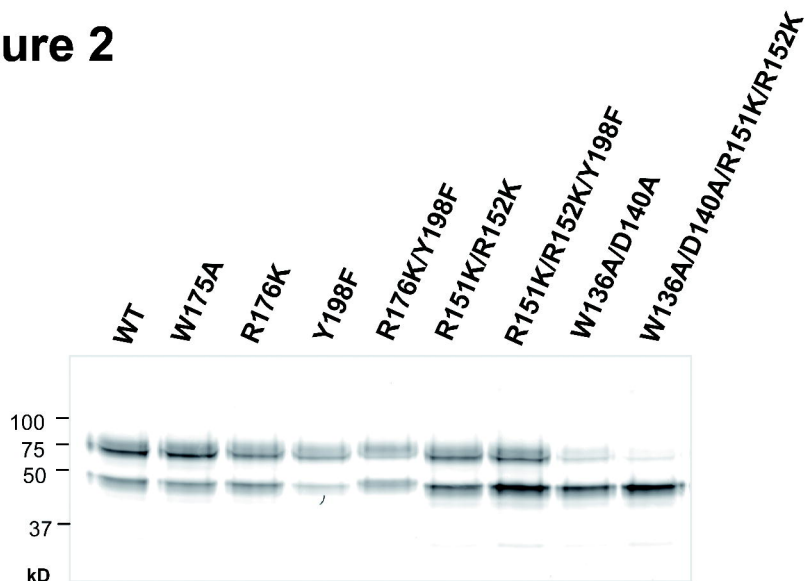
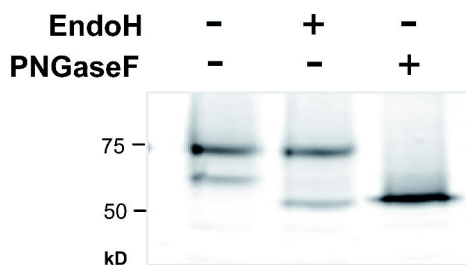


Figure 2

A



B



C

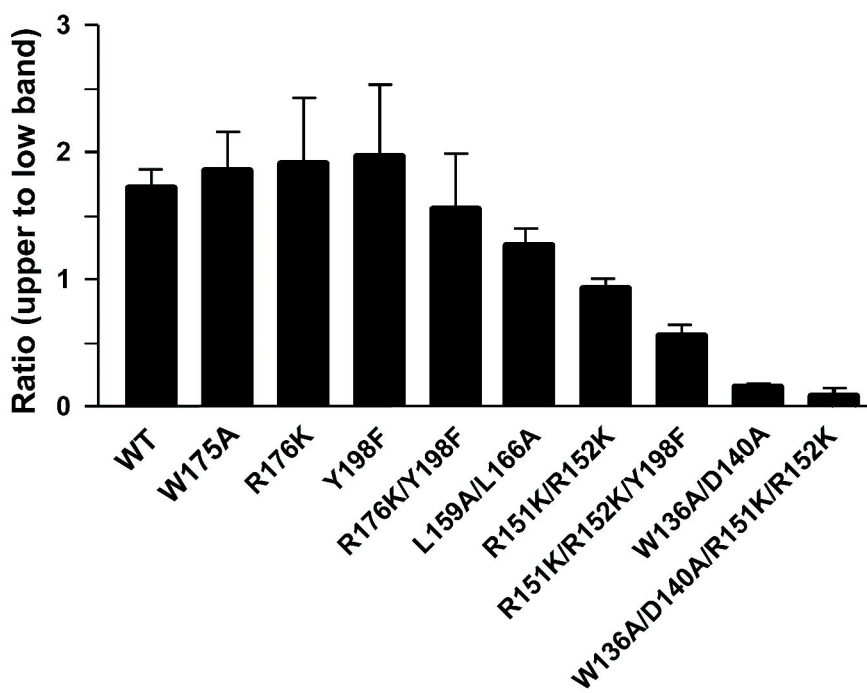


Figure 3

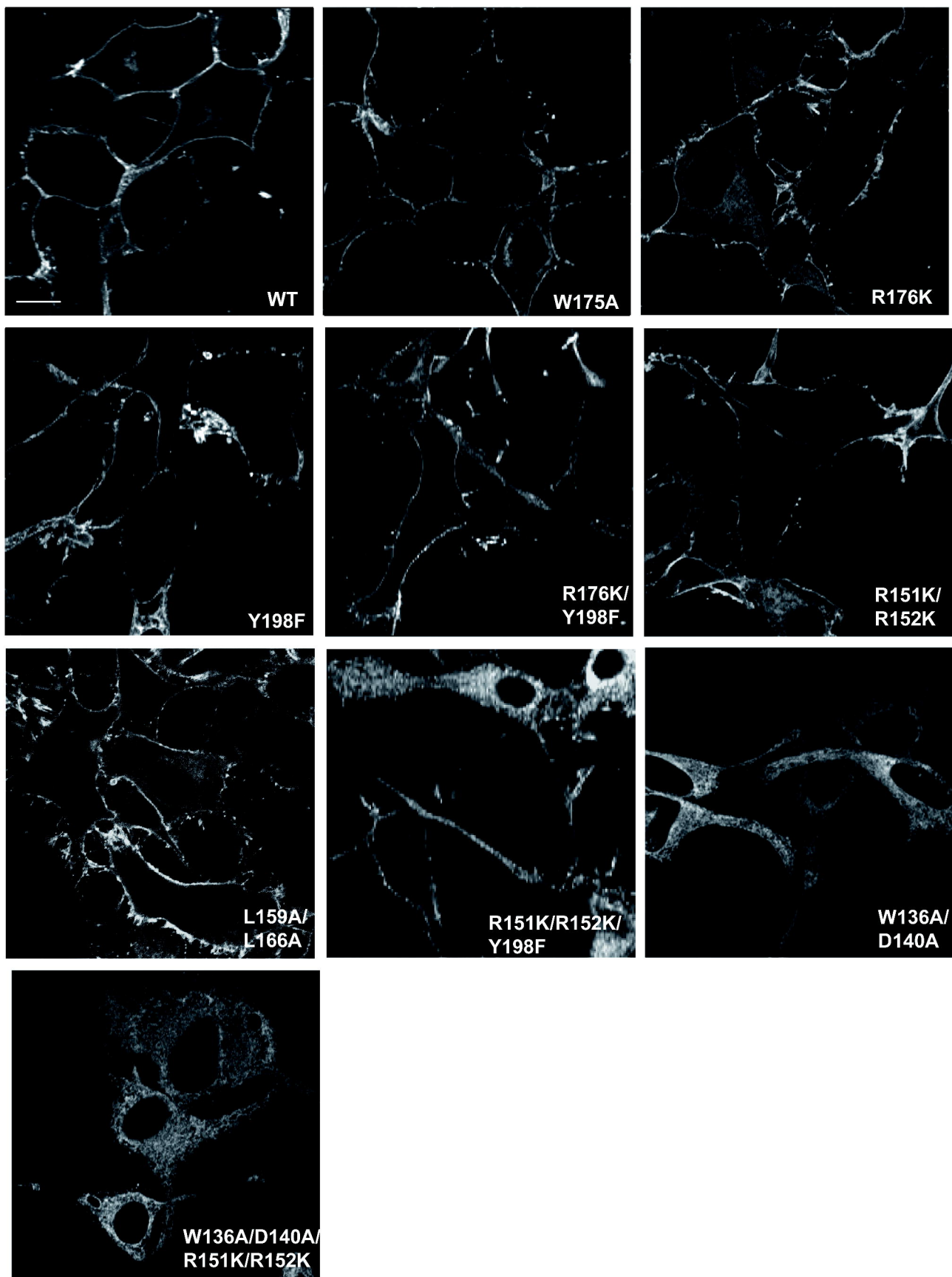


Figure 4

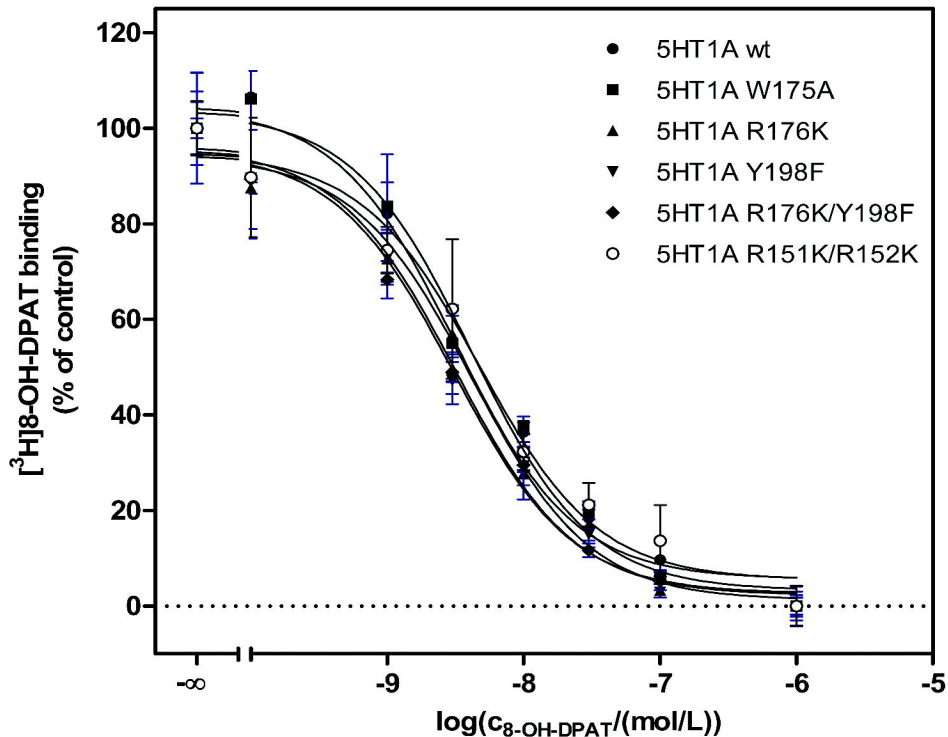


Figure 6

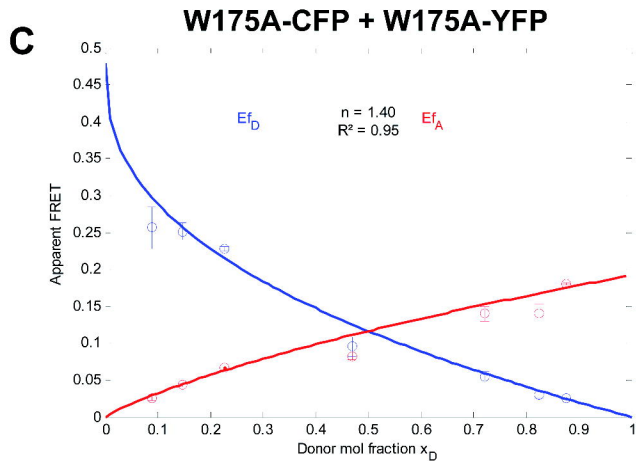
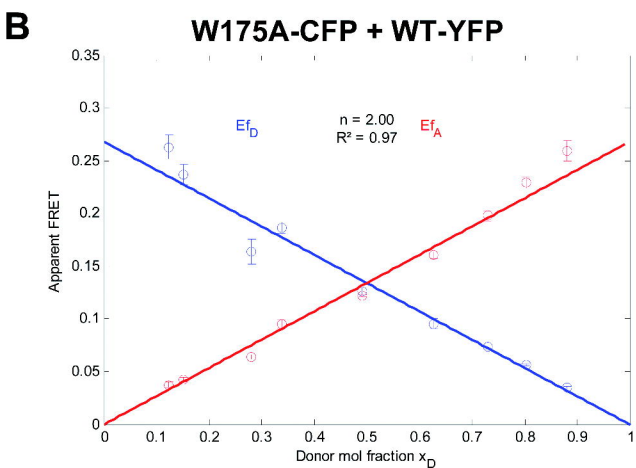
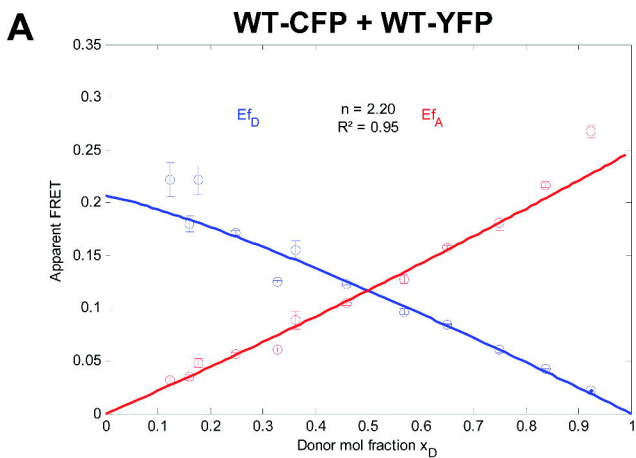
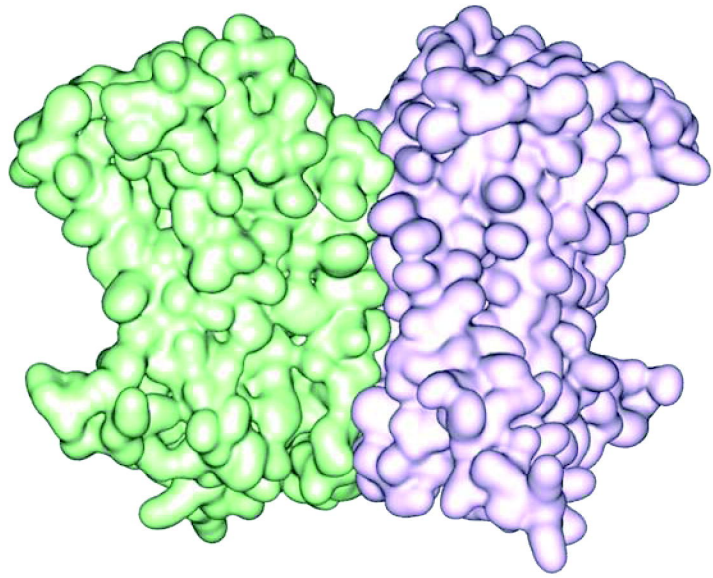


Figure 7

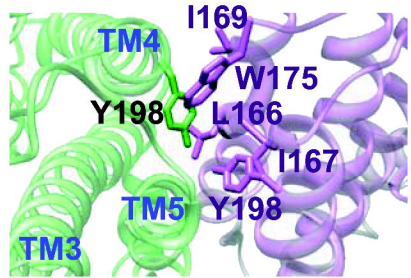
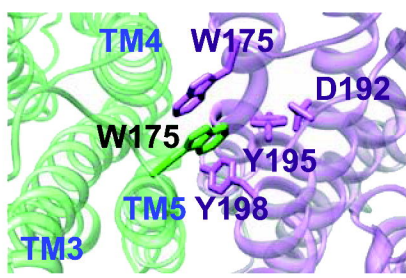
Monomer I

Monomer II

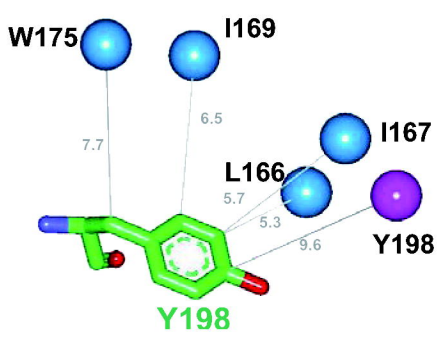
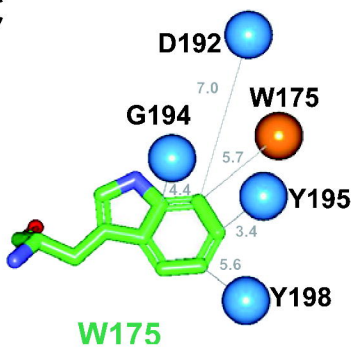
A



B



C



- Aromatic + van der Waals
- Van der Waals
- Hydrogen bond